Development of GEM tracker for in-medium $\phi \to e^+e^-$ measurement

Yusuke Komatsu

University of Tokyo

Master's Thesis

February 7, 2011

Contents

1 Introduction **4**
1.1 Physics Motivation 4
1.1.1 Origin of mass 4
1.1.2 Existing experimental results 4

2 J-PARC E16 experiment **11**
2.1 Overview 11
2.2 Spectrometer of E16 experiment 12
2.2.1 Gas Electron Multiplier(GEM) tracker 12
2.2.2 Hadron Blind Detector 15

3 GEM Tracker **16**
3.1 Configuration of GEM 16
3.1.1 Mechanical structure 16
3.1.2 GEM chamber 17
3.2 Manufacturing of large GEM 21
3.2.1 Alignment of the holes 21
3.2.2 Flabbiness of large GEM 24
3.3 Gain measurement of large GEM 27
3.3.1 Setup 27
3.3.2 Results and conclusions 28

4 E16 simulation **32**
4.1 Purposes 32
4.2 Procedure of simulation 34
4.3 Mass resolution as a function of position resolution 38
4.3.1 inclined electrons 38
4.3.2 Vertical position resolution 44
4.4 Other parameter dependence 46
4.4.1 Vertex reconstruction 46
4.4.2 Magnetic field 47
4.5 Conclusion 51

5 Beamtest **52**
5.1 Purposes 52
5.2 Beam line 53
5.3 Test setup 54
5.4 Analysis procedure 55
5.4.1 SSD analysis 55

5.4.2 GEM analysis 62
5.4.3 Additional cut 65
5.4.4 GEM hit position analysis 69
5.4.5 GEM efficiency calculation 74
5.5 Results 74
5.5.1 Operation of large GEM 76
5.5.2 Position resolution and efficiency 79
5.5.3 Resolution of the bottom side 85
5.5.4 Analysis without waveform information 87

5 Conclusions & Outlook **92**

Abstract

A particle tracker using gas electron multiplier (GEM) is developed for J-PARC E16 experiment. Especially, the performance of large size GEM such as 200×200 mm^2 and 300×300 mm^2, and the readout configuration of the tracker is studied. As a result of beamtest, large GEM had position resolution less than 100 μm for 0° beam, and a strip readout of 350 μm pitch achieved the position resolution of $\sim$100 μm for up to 15° inclined beam. These results fulfill the requirements expected from the Monte-Carlo simulation of the E16 experiment.

1 Introduction

An experiment is proposed at J-PARC which is a high intensity proton accelerator in Japan to study the origin of hadron mass. The experiment is named J-PARC E16.

1.1 Physics Motivation

The experiment aims to study the mechanism of hadrons obtaining its mass. This mechanism is explained theoretically as the spontaneous symmetry breaking(SSB) proposed by Prof.Nambu[1][2]. SSB is an essential concept of physics and many experiments have tried to understand the details of the mechanism.

1.1.1 Origin of mass

In the standard model, quark acquires its mass at two stages. The first is the spontaneous breaking of electro-weak symmetry, in which the Higgs field has non-zero expectation value. The second is the spontaneous breaking of chiral symmetry, in which quark-anti quark condensates due to strong interaction.

The mass generated by Higgs mechanism is expected to be only $\sim$2 MeV/c^2 for u-quark, so over 99% of the constituent quark mass is caused by the spontaneous breaking of chiral symmetry. So it is important to know the mechanism of chiral symmetry breaking to understand the origin of mass.

In hot and/or dense matter, like the intial state of the universe, chiral symmetry is partially restored and the properties of hadrons are expected to change accordingly. Therefore, in-medium properties of hadrons can be used as good probes to understand the origin of mass.

Several experiments have been performed to study the hadron property in hot and/or dense medium.

1.1.2 Existing experimental results

Several experiments are performed to study the hadron property in hot and/or dense medium. Two experiments, KEK-E325 and JLab-CLAS G7 have significant results.

KEK-E325 experiment

KEK-E325 experiment is conducted at KEK 12GeV proton synchrotron to study the in-medium property of light vector mesons, $\rho/\omega/\phi$. The order parameter of chiral symmetry breaking is the vacuum expectation value of quark-anti quark condensates $< \bar{q}q >$, but $< \bar{q}q >$ is not observable. Instead, the mass of vector meson is predicted to change in dense matter [4] due to the patial restoration of chiral symmetry. So the invariant mass spectra of $\rho/\omega/\phi \to e^+e^-$ and $\phi \to K^+K^-$ in nuclear medium are measured in KEK-E325 experiment. Spectrometer of the E325 experiment is shown in Fig. 1. As results, 9% decreasing mass was observed for ρ and ω meson, but there is no width broadening[5] (Fig. 2). In addition, 3.4% of decreasing of ϕ mass and a factor of 3.6 of width broadening is observed at normal nuclear density[6] (Fig. 3).

A spectrometer is constructed to detect lepton pairs from slowly moving mesons which have larger probability to decay inside nucleus. Leptons are free from final interaction but branching ratio for e^+e^- channel is low ($10^{-4} \sim 10^{-5}$). To overcome this disadvantage, high intensity beam of 10^9 protons per spill is used.

As targets C and Cu are used and each interaction length is 0.21% and 0.054% respectively[5]. As for ρ/ω mass region, significant excess is observed only lower side of the ω peak in the mass spectra. Higher mass side is reproduced by the known hadronic decay sources. By a model calculation with mass shift of $m(\rho)/m(0) \sim 1-k(\rho/\rho_0)$, they conclude that mass of ρ meson decreases 9% at normal nuclear density. Here ρ_0 is the normal nuclear density and m(0) is the mass in free space. From the absence of a tail in higher side, no width broadening is reported.

In the mass spectra of ϕ mass region, significant excess is observed in the lower side of ϕ peak only in the case of Cu target and $\beta\gamma$ of ϕ <1.25. This is consistent with an expectation. Only slowly moving ϕ meson can decay in nucleus. The lifetime of ϕ is long ($c\tau \sim$46fm) compared to the size of nucleus. Thus excess is likely observed at large nuclear target and slowly moving ϕ. Mass decreasing of 3.4% and a factor 3.6 of width broadening are derived by a mode calculation with proportional term to ρ/ρ_0.

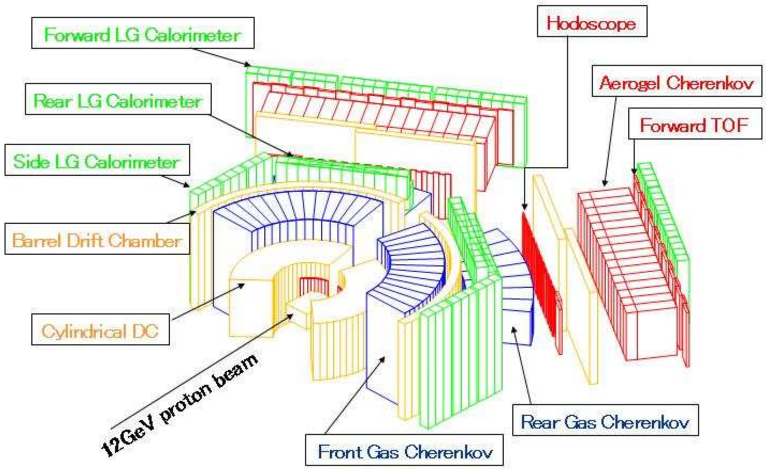

Figure 1: Schematic view of the spectrometer of E325 experiment

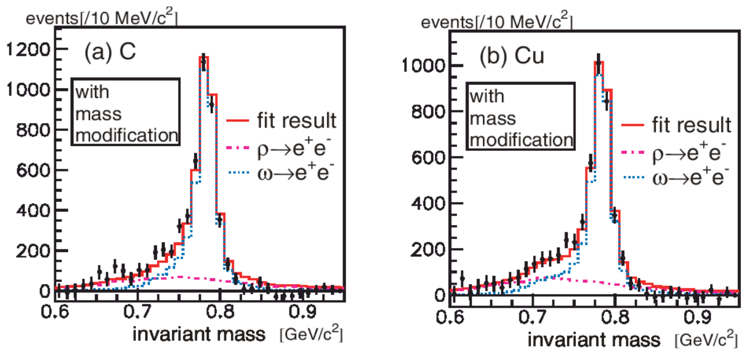

Figure 2: Obtained spectra of ρ/ω meson in the E325 experiment. (left) C target., (right) Cu target.[5]

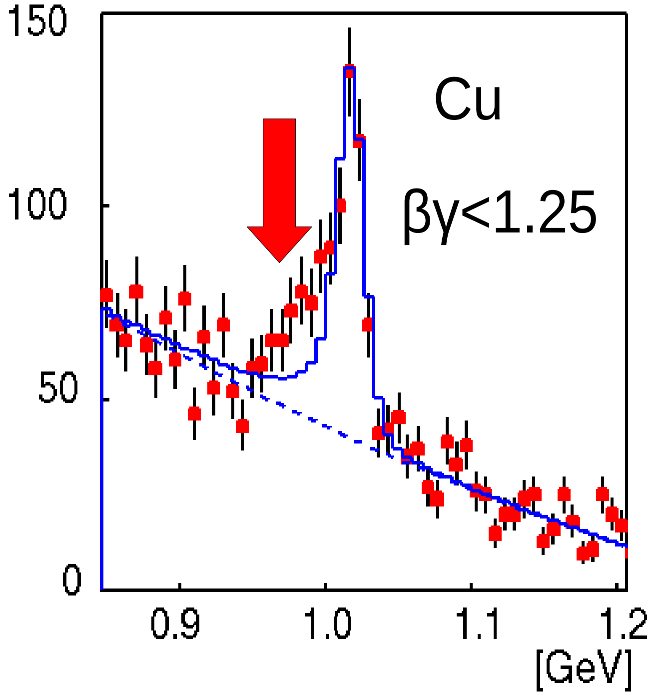

Figure 3: Obtained spectra of ϕ meson in the E325 experiment. Excess is observed in Cu target and $\beta\gamma_\phi < 1.25$.[6]

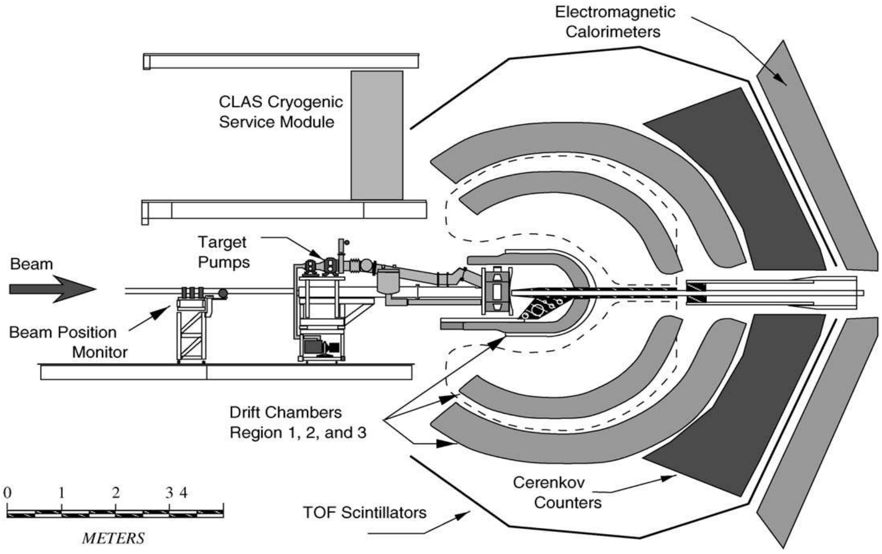

Figure 4: Schematic view of CLAS detector[7]

J-Lab g7 experiment

CLAS g7 experiment at Jefferson Laboratory measures the medium modification of ρ meson. The g7 experiment states the upper limit of the mass shift of ρ meson as 5.3% under normal nuclear density and no modification beyond nuclear many body effects is observed. This is inconsistent with the results of E325 experiment which reports 9% mass decreasing of ρ/ω meson.

The reaction of $\gamma + A \rightarrow (\rho, \omega, \phi) + A^*$ is used in the g7 experiment to generate vector mesons in nuclear medium. If $A + A$ reaction, the results contain the effects from wide range of density and temperature in the reaction, so it becomes difficult to derive a parameter of mass modification which couple to density or temperature. On the other hand, generating vector meson in nuclear medium by fixed target experiment is clearer since zero temperature and normal nuclear density is achieved.

(**vector meson**) $\rightarrow e^+e^-$ is detected to reconstruct mass. The CEBAF Large Acceptance Spectrometer(CLAS) which covers $8° < \theta < 142°$ and 80% in azimuth for charged particles is built for the measurement(Fig. 4). Used targets are liquid-deuterium, C, Ti and Fe. Cherenkov counters and electromagnetic calorimeters in the foward are the main parts for electron idetification and pion rejection.

The obtained spectra are shown in Fig.5. The background of e^+e^- pairs from uncorrelated sources are subtracted and it is estimated by event mixing method. The calculation for the spectra is done by Boltzmann-Uehling-Uhlenbeck(BUU) transport model[9] which contains the final-state interactions for produced particles in the nucleus. Then the calculated spectra for $\omega \to e^+e^-$, $\omega \to \pi^0 e^+e^-$ and $\phi \to e^+e^-$ are subtracted because ω and ϕ meson have long lifetimes and the probability to decay in nucleus is small. The results of ρ meson is Fig. 6. The ρ meson spectra are fitted with the calculation very well. The width of spectra are consistent with the natural width and collisional broadening effect which is included in BUU model. Mass shift parameter α which is defined as

$$\frac{m_{VM}(\rho)}{m_{VM}(\rho = 0)} = 1 - \alpha \frac{\rho}{\rho_0}$$

is $\alpha = 0.02 \pm 0.02$ for Fe-Ti target. As a result systematic error $\Delta\alpha = \pm 0.01$ is added and an upper limit of $\alpha = 0.053$ with a 95% confidence level is concluded. This is inconsistent with the results of KEK E325 expriment.

The g7 experiment measured the spectrum of ϕ meson too, but ϕ meson is not studied due to the low statistics. And the momentum dependence of in-medium modification is not still made clear. More systematic measurement such as studying momentum dependence and target nuclear size dependence of modification is awaited.

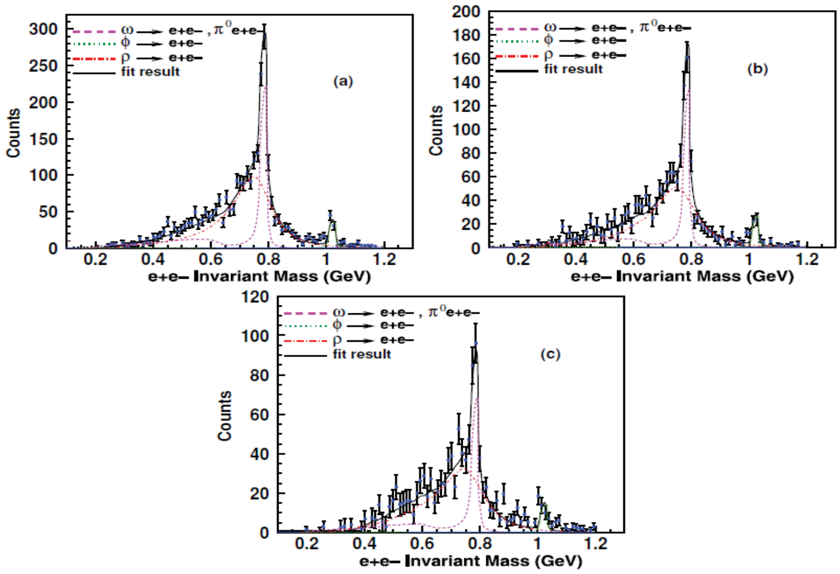

Figure 5: Obtained spectra by the J-Lab g7 experiment. (a) ^{2}H target, (b) C target, (c) Fe-Ti target. Background is subtracted.[8]

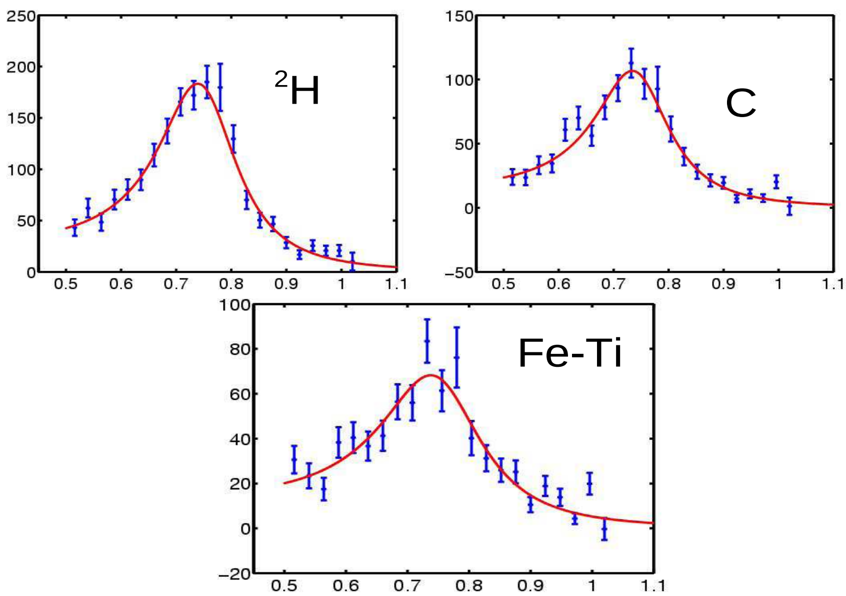

Figure 6: Obtained ρ meson spectra. (top left) ^{2}H target., (top right) C target., (bottom) Fe-Ti target.[10]

2 J-PARC E16 experiment

In this section, the details of J-PARC E16 experiment are explained.

2.1 Overview

The J-PARC E16 experiment focuses on detecting e^+e^- pair from the decay of vector mesons in nuclear medium, especially for ϕ meson. The advantages of using $\phi \to e^+e^-$ are the followings.

- There is no other resonance near ϕ meson and ϕ meson has relatively narrow width of 4.26 MeV/c^2. So it is suitable for the measurement of mass shift and width broadening. Here, ρ and ω mesons are also candidates, however their mass spectra overlap and it is difficult to have clear separations.

- Lepton pairs can avoid the effects of strong interaction. It is expected that measured e^+e^- maintain the information of ϕ at decay.

However, there are also difficulties.

- The lifetime of ϕ is long and $c\tau$ is $\sim$46 fm [6]. This is longer than the typical size of nucleus, $\sim$10 fm. This means that the probability for generated ϕ meson to decay in nucleus is small.

- The branching ratio of e^+e^- decay is $\sim 10^{-4}$.

To overcome these difficulties, we are planning to have a high intensity beam and large acceptance spectrometer. At J-PARC, the beam of 10^{10} protons per spill is available. We build large acceptance and high mass resolution spectrometer. Simulation results of mass distribution with different mass resolutions are shown in Fig. 7. Mass resolution of 5 MeV/c^2 is required to recognize clear mass modification.

These upgraded experimental apparatus enable us to study the modification of hadron mass spectra more systematically. At J-PARC, 100 times larger statistics can be collected and we can study the dependence of mass spectrum on nuclear size and the momentum($=\beta\gamma$) of ϕ meson. We use the targets of A=1$\sim$200.

The goal is to derive the dispersion relation between mass and momentum of vector meson.

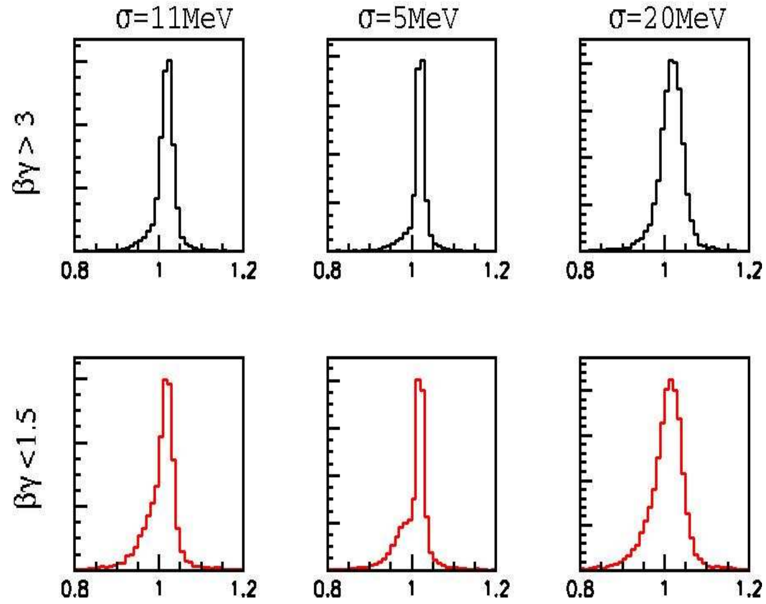

Figure 7: Simulation of mass distribution[11]

2.2 Spectrometer of E16 experiment

Figure. 8 and Fig. 9 show the schematics of the experimental setup. The spectrometer consists of GEM tracker, Hadron Blind Detector (HBD), pad chamber and PbGl calorimeter.

GEM tracker is used to determine the momentum of charged particles. HBD is a Cherenkov detector and used for electron identification together with PbGl calorimeter. Pad chamber is for pattern recognition. GEM tracker and HBD are explained in detail in the following sections.

2.2.1 Gas Electron Multiplier(GEM) tracker

Tracker measures the path of charged particles to reconstruct their momentum. In the E16 experiment, Gas Electron Multiplier(GEM) is used to detect the hit positions. Ionization in gas by charged particles is utilized to detect their tracks. Then, ionized electrons need to be amplified to be read out with electronics. The amplification process is done by GEM. GEM has many small holes and the potential in the holes make avalanche of electrons. More detail is described in chapter 3.

Hit position is determined by two dimensional readout strips. One unit of tracker has three GEM chambers at three different radius, so three points of the track can be measured in magnetic field. Each chamber is put at radius of 200 mm, 400 mm and 600 mm. For example, one of the main reason for adopting GEM is its rate capability. Counting rate of $\sim$5 kHz/mm^2 is expected due to the interactions between the beam halo and the material around beam pipe[11]. We have to make fine cells to cope with such high rate counting. if drift chamber is used with this rate, cell size should be 0.7 mm$\times$100 mm. There are many difficulties to have large acceptance with such very small pitch wires. On the other hand, GEM is operated in COMPASS experiment up to 25 kHz/mm^2[12]. Therefore, GEM is a suitable tool for high rate environment.

The required position resolution is about 100 μm, which is discussed in chapter 4 and 5.

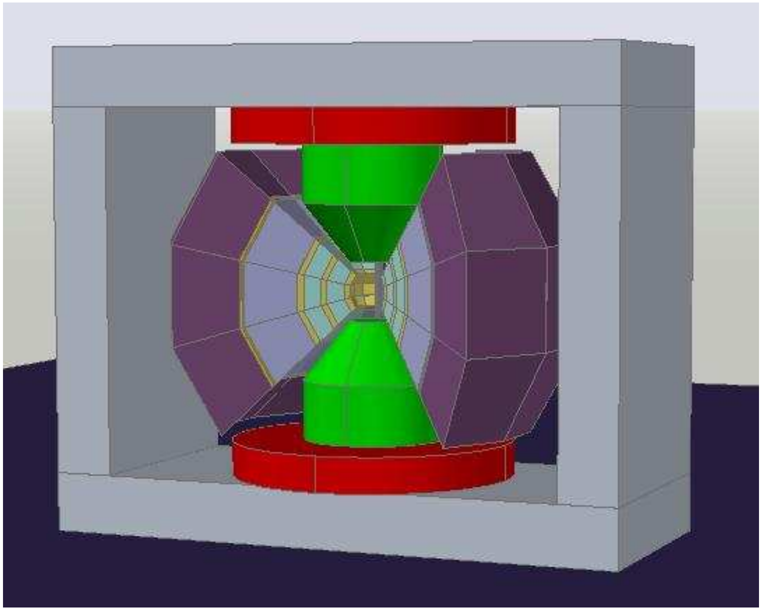

Figure 8: Spectrometer overview

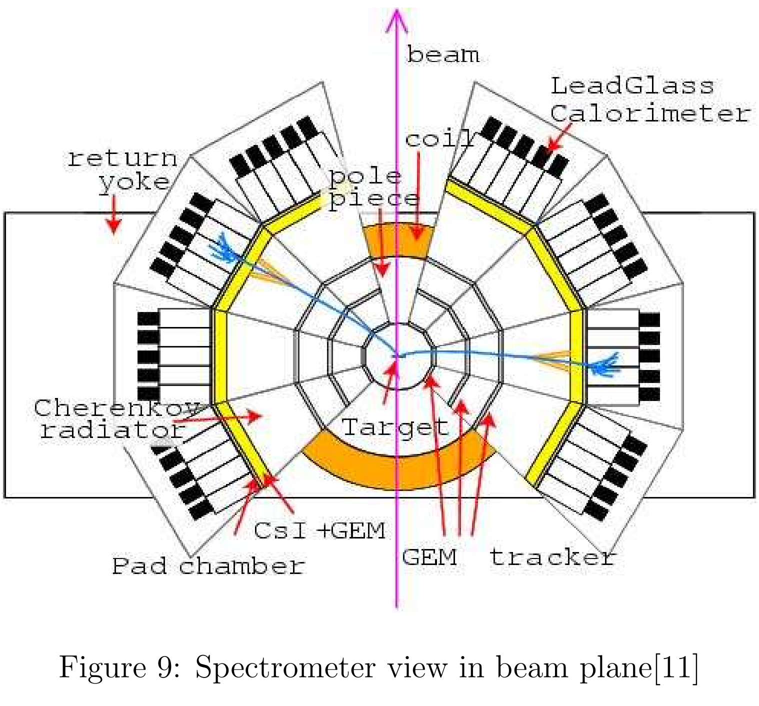

Figure 9: Spectrometer view in beam plane[11]

2.2.2 Hadron Blind Detector

Another spectrometer component is hadron blind detector (HBD). HBD is gas Cherenkov detector for electron identification and developed in PHENIX experiment at BNL[13]. CsI photo-cathode is formed by deposition on the surface of the top GEM as shown in Fig. 10. Both radiator gas and amplification gas are common and CF_4 gas is used. The electric potential of cathode mesh is a lttle higher than the top GEM. Then, ionized electrons move toward to cathode mesh, while photo-electrons emitted by Cherenkov light are brought in GEM for amplification and transportation to the readout.

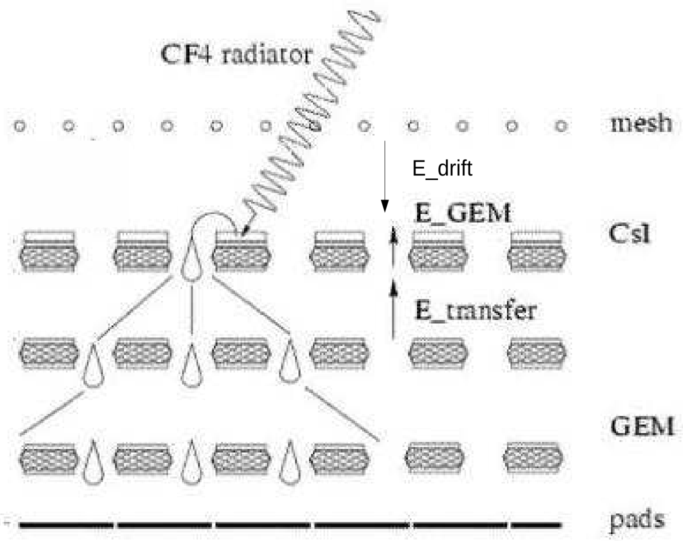

Figure 10: The mechanism of HBD. [14]

3 GEM Tracker

3.1 Configuration of GEM

3.1.1 Mechanical structure

Gas Electrons Multiplier (GEM) is a kind of micro pattern gas detectors (MPGDs) and invented at CERN[15]. GEM is composed of a thin insulator sandwiched by metal layers which have thickness of 4∼5 μm, and there are many small holes. The diameter of a hole is approximately 70 μm and hole pitch is 140 μm. GEM is operated in gas and high voltage of 350V is applied. Such high voltage makes a strong electric field in the holes and ionized electrons are amplified in the hole. GEM is proposed to be used for a tracker and a Cherenkov detector in E16 experiment for electron amplification.

The advantages of GEM are,

- High gain can be obtained by stacking GEM. Gain of 10^4 can be achieved and is our requirement.
- Two dimensional information of a hit position is obtained using perpendicular strips as a readout.
- GEM has a high rate capability. COMPASS experiment at CERN used GEM as a tracker and achieved ∼70 μm position resolution up to 25 kHz/mm^2[12]. In E16 experiment, 5 kHz/mm^2 is the expected.

Three GEM foils are stacked in a chamber in our configuration. Designed values of GEM are shown in Table. 1. GEM is manufactured by wet etching. Copper and polyimide are etched by chemicals to make holes. So the shape of a GEM hole becomes double-conical shape because of the penetration of chemicals. The metal layer of a large GEM are divided into several segments in case of large area GEM to decrease the capacitance. Large capacitance causes serious damage, when it is accidentally discharged. The size of 200×200 mm^2 GEM are divided into 4 segments and 300×300 mm^2 GEM are into 12 segments.

thickness[μm]	metal diameter[μm]	hole diameter[μm]	hole pitch[μm]
50	75	40	140

Table 1: The designed value of GEM

<table>
<tr><th>thickness [μm]</th><th>x-strip width [μm]</th><th>y-strip width [μm]</th><th>strip pitch [μm]</th><th>polyimide</th></tr>
<tr><td rowspan="3">25</td><td>70</td><td>290</td><td>350</td><td>leave</td></tr>
<tr><td rowspan="2">140</td><td rowspan="2">580</td><td rowspan="2">700</td><td>leave</td></tr>
<tr><td>remove</td></tr>
</table>

Table 2: The configuration of a readout board

Three types of readout boards are prepared and they are shown in Table. 2. Readout boards consist of perpendicular strips called x-strips and y-strips. The x-strips are placed on the top side as shown in Fig. 11. The width of a x-strip is 70 μm and y-strip is 290 μm. The width of a y-strip is larger because y-strips are partially screened by x-strips. The Readout strips are manufactured on both sides of polyimide foil which has 25 μm thickness. So there remains polyimide between x-strips and y-strips.

Two types of readout are prepared about the polyimide between x-strips and y-strips. One leaves the polyimide. In the other type, the polyimide above y-strips is removed. The latter is expected to be better to read signals than the former because the pulse height would be higher. But if the former was enough for the experiment's requirement, the cost is reduced.

The strip pitch is also considered of two types. One is 350 μm pitch and the other is 700 μm pitch. 700 μm pitch is achieved by combining every two strips of the 350 μm pitch readout. The comparison of the 350 μm pitch and 700 μm pitch was done at the beamtest.

3.1.2 GEM chamber

The configuration of a GEM chamber is shown in Fig. 11. In this study, three GEM foils are used to get $\sim 10^4$ of gain. Mesh is a cathode and the readout is an anode. The radiation length of a GEM chamber is summarized in Table. 3.There are three kinds of the gaps called drift gap, transfer gap and induction gap from the top to bottom. High voltage is applied to the mesh and three GEM foils by a register chain.

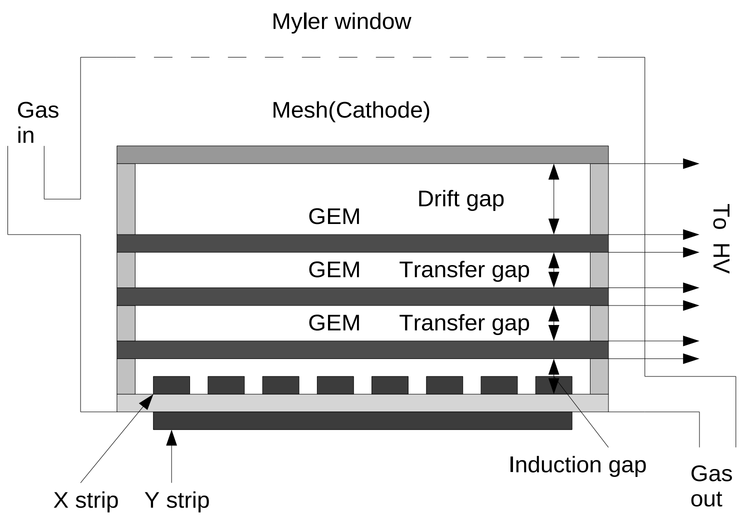

Figure 11: Schematic view of a GEM chamber

name	component	X_0/Density[cm]	length[μm]	aperture ratio[%]	radiation length[%]
GEM	window myler	28.5	25		0.0088
	cathode	8.90	25		0.0281
	copper	1.44	24	26.3	0.123
	kapton	28.6	150	7.47	0.0486
Readout	copper-x	1.44	4	80	0.0056
	copper-y	1.44	4	17.1	0.0231
	kapton	28.6	25		0.0087
total					0.246

Table 3: The radiation length of a GEM chamber

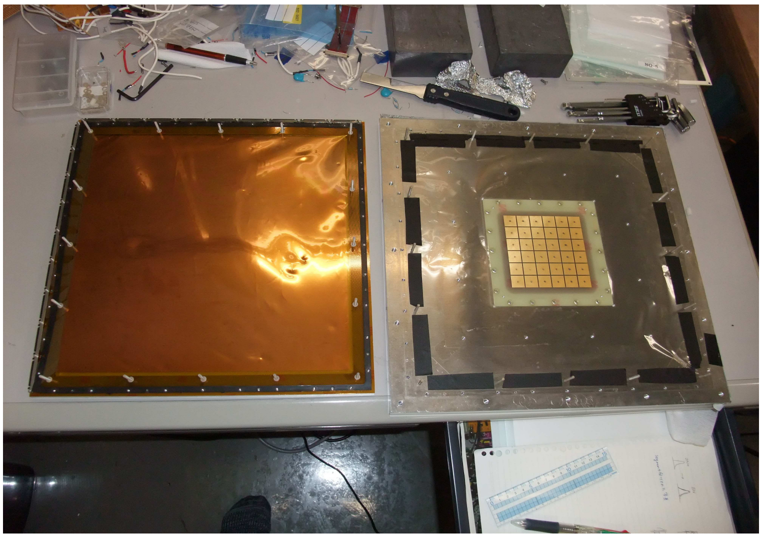

Figure 12: Readout board :(left) strip readout, (right) pad readout

Figure 13: GEM chamber: (left) 100×100 mm^2, (middle) 200×200 mm^2, (right) 300×300 mm^2

3.2 Manufacturing of large GEM

200×200 mm^2 and 300×300 mm^2 GEM are developed for a tracker. Large size GEM has 2 problems in manufacturing, one is hole size and the other is the flabbiness of the foil.

3.2.1 Alignment of the holes

The hole size is determined by the alignment of the masks in both side. The pattern of the mask is copied on the photo-resist by exposing light (Fig. 14). The light changes the solubility of the photo-resist against the developer.

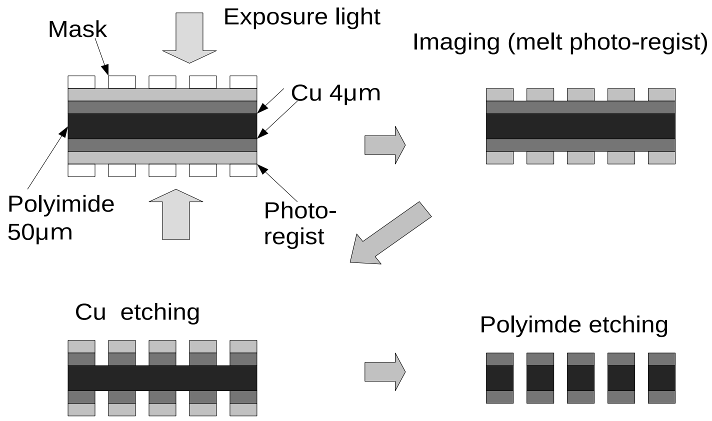

Figure 14: Making process of GEM

If there is a misalign between the top mask and the bottom mask, the shape of holes results in cat's eye shape (Fig. 15). As a result, the hole size of the top side or the bottom side becomes larger for trimming the shape the hole.

It is more difficult to align the masks accurately as the size of GEM becomes larger. The hole size of 100×100 mm^2 GEM and 300×300 mm^2 are shown in Table. 4 and 5. The hole size of 300×300 mm^2 GEM is larger than 100×100 mm^2 due to misalignment.

First, we tried to solve this problem by making the hole size of the bottom larger than the accuracy of the alignment. But it degrades the gain because the field is weakened in the larger holes. So the way to improve the alignment accuracy of the masks without changing the hole size was considered.

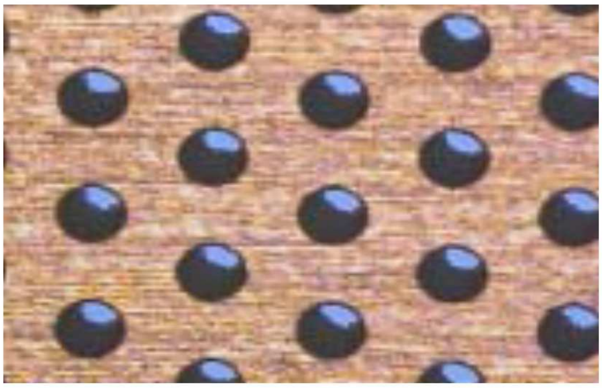

Figure 15: The hole shape of GEM :top mask and bottom mask are misaligned.[17]

As a solution, a mask which has the top side the bottom side together is developed. By this idea the metal diameter of $\sim$77 μm and the polyimide diameter of $\sim$50 μm are achieved (Table. 6).

region	A				B				C				D				E			
Cu or PI	Cu		PI		Cu		PI		Cu		PI		Cu		PI		Cu		PI	
direction	X	Y	X	Y	X	Y	X	Y	X	Y	X	Y	X	Y	X	Y	X	Y	X	Y
average[μm]	74	77	50	46	71	78	48	44	77	75	47	48	74	77	49	45	76	79	47	50

Table 4: An example of hole size of 100×100 mm^2 GEM [18]

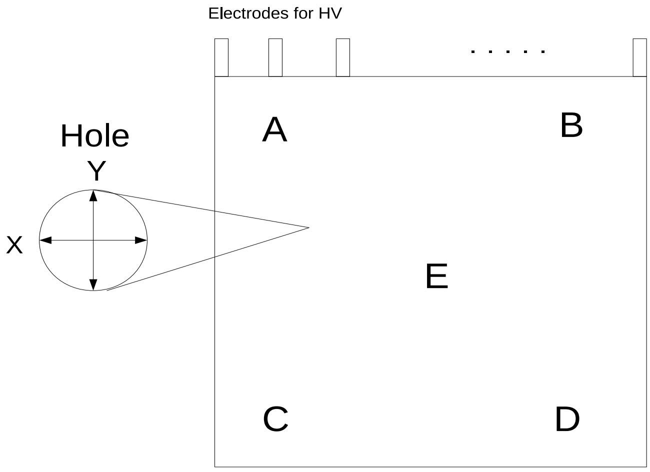

region	A				B				C				D				E			
Cu or PI	Cu		PI		Cu		PI		Cu		PI		Cu		PI		Cu		PI	
direction	X	Y	X	Y	X	Y	X	Y	X	Y	X	Y	X	Y	X	Y	X	Y	X	Y
average[μm]	84	84	56	54	85	85	55	52	84	85	53	53	84	84	59	53	84	84	54	54

Table 5: An example of hole size of 300×300 mm^2 GEM before alignment is improved [18]. PI means the polyimide. 17 holes are sampled in each region A, B, C, D and E.

region	A				B				C				D				E			
Cu or PI	Cu		PI		Cu		PI		Cu		PI		Cu		PI		Cu		PI	
direction	X	Y	X	Y	X	Y	X	Y	X	Y	X	Y	X	Y	X	Y	X	Y	X	Y
average[μm]	75	75	48	53	77	76	47	54	77	76	49	54	78	78	49	51	76	76	48	53

Table 6: An example of hole size of 300×300mm^2 GEM after alignment is improved [18].

3.2.2 Flabbiness of large GEM

Flabbiness is another problem in developing large GEM. The length of transfer gap of GEM is 2 mm in our configuration. At the first attempt of manufacture, this gap can't be kept because large GEM touch with each other and short in transfer gap due to its flabbiness. The gain depends on the field in the transfer gap, so this problem also leads to the degradation of gain.

The flabbiness of large GEM is expected to be solved by the tension with which GEM is fixed to its frame. So a jig which pulls GEM equally is developed (Fig. 16).

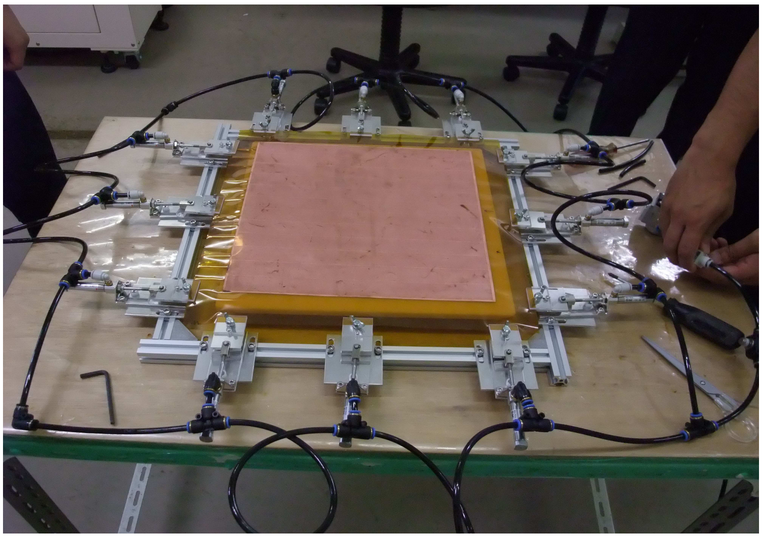

Figure 16: The jig for pulling GEM

This jig has 12 air cylinders and the tension can be controlled. And a new frame which is 1.5mm thickness is prepared.

The relative flabbiness is measured by a measuring machine with laser at Rinei.Co. (Fig. 17). GEM foil is pulled with 0.2, 0.25 and 0.35MPa/cyliner by the jig and fitted with frame. Then GEM is fixed to a board and the relative flabbiness is measured. The results are shown in Fig. 18, 19 and 20. X axis and y axis corresponds to the sides of GEM. The zero point in the figures is the max value among the measured lengths.

The edge of GEM seems higher than the center part for all the measurements, so it may be some problem of a base board or else. But the ununiformity of GEM is improved in 0.25 MPa and 0.35 MPa than 0.2 MPa about 500 μm. From these results, it is determined to pull GEM with 0.25MPa/cylinder when fit to frame.

Figure 17: Measurement of GEM flabbiness.

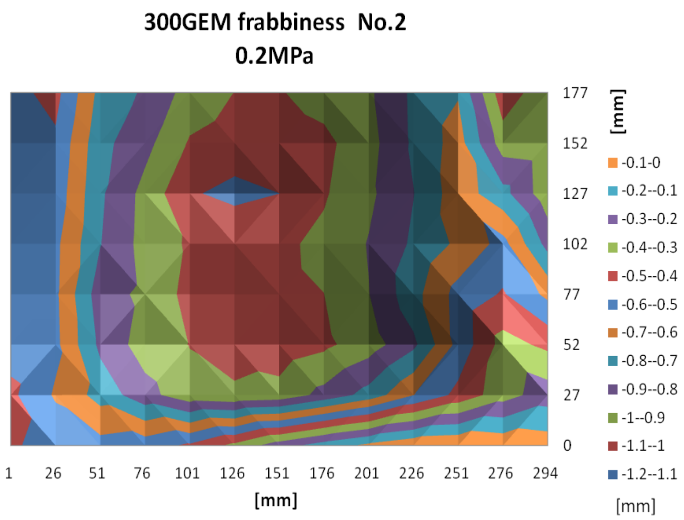

Figure 18: The flabbiness of GEM pulled with 0.2MPa.

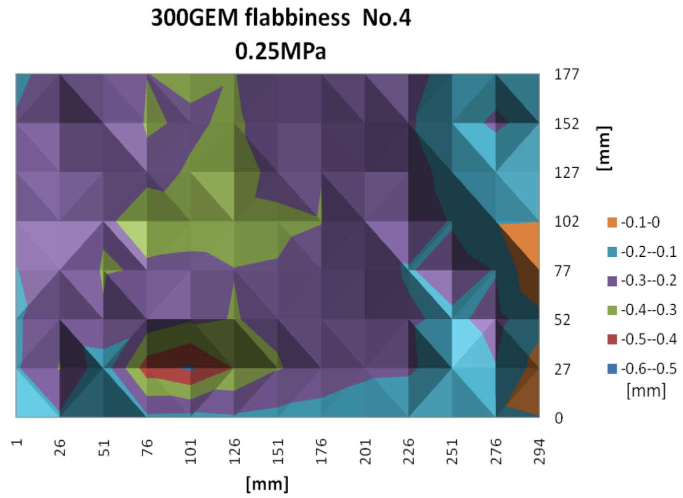

Figure 19: The frabbiness of GEM pulled with 0.25MPa.

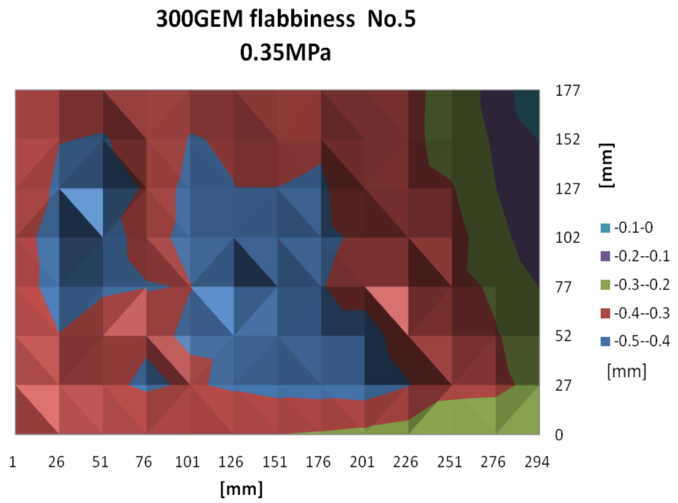

Figure 20: The flabbiness of GEM pulled with 0.35 MPa.

3.3 Gain measurement of large GEM

The gain of large GEM is evaluated by laboratory test.

3.3.1 Setup

The setup is shown in Fig. 21. Pure Ar(99.999%) and pure CO_2(99.99%) are mixed to Ar-70% CO_2-30% . $ArCO_2$ is kept flowing during the measurement.

5.9 KeV characteristic-X ray of Fe^{55} is used as a reference peak. Signal charge is detected by a pad electrode whose size is 1.5×1.5 cm^2. Then signal is amplified by integral amp whose gain is 1 V/pC and time constant is τ=1 μs (Fig. 22).

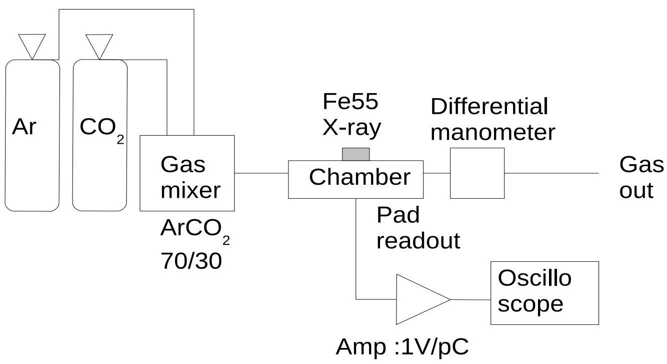

Figure 21: Setup for gain measurement

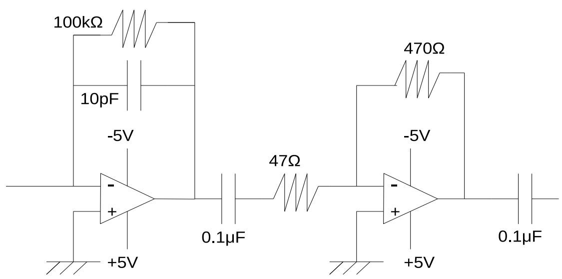

Figure 22: Schematic figure of integral amp

The working function of Ar and CO_2 is 26 eV and 33 eV[16], so the working function of $ArCO_2$ 70/30 is,

$$26 \times 0.7 + 33 \times 0.3 = 28.1eV$$

Thus the number of electrons generated by 5.9keV X-ray is,

$$5900/28.1 \sim 210$$

If the pulse height was x [mV], the effective gain is calculated as following,

$$(\textbf{Effective gain}) = \frac{x \times 10^{-3} \times 10^{-12}}{1.6 \times 10^{-19} \times 210}$$

10^{-12} [C/V] indicates the gain of the preamp and 1.6×10^{-19} is the electric charge of electron.

3.3.2 Results and conclusions

Effective gain is measured about 100×100 mm^2, 200×200 mm^2 and 300×300 mm^2 GEM. The results are shown in Fig. 23.

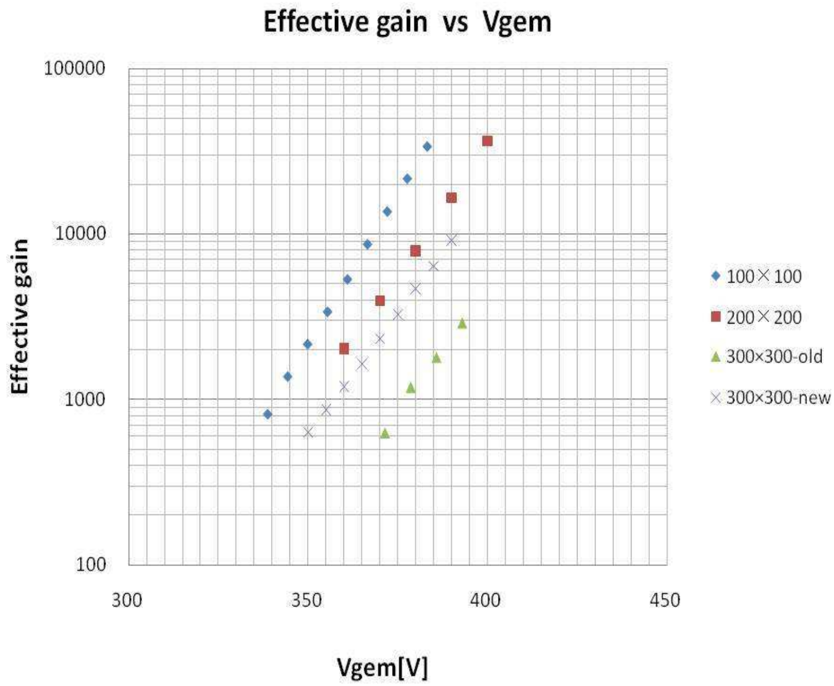

Figure 23: The comparison of gain measurement: '300×300-old' indicates the 300×300 mm^2 GEM before the improvement of the hole size and the flabbiness. '300×300-new' is after improved.

The configuration of the electric field for each measurement is slightly different and it causes a difference between each other. The detailed configuration is shown in Table. 7.

	GEM size [mm^2]			
	100×100	200×200	300×300-old	300×300-new
Drift gap [mm]	6	6	3	6
Transfer gap1 [mm]	3	3	3.5	2
Transfer gap2 [mm]	3	3	3.5	2
Induction gap [mm]	3	2	2.5	2
E_D [kV/cm]	0.6	0.6	1.17	0.6
E_{T1} [kV/cm]	2.55	2	1.31	1.95
E_{T2} [kV/cm]	2.55	2	1.31	1.95
E_I [kV/cm]	2.55	4	3.93	3.9

Table 7: The configuration of gap length [mm] and electric field [kV/cm] of each measurement. The field strength shown are at V_{GEM} =383, 400, 393, 390 V for each.

The gain of 300×300 mm^2 GEM is different factor ∼4 between old one before the improvement of hole size and flabbiness and new one after improvement. According to the measurements in [19], the difference which comes from the electric field is estimated as in Table. 8.

gap	old [kV/cm]	new [kV/cm]	gain factor (new/old)
Drift	1.17	0.6	0.97
Transfer	1.31	1.95	2.13
total			2.07

Table 8: Estimated factor which comes from the strength of the field.

About factor 2 increasing of gain is due to the electric field and remaining factor 2. This is considered to be due to the improvement of the hole size. The metal and polyimide hole diameter of the old 300×300 mm^2 GEM is ∼84 μm and ∼53 μm. On the other hand, ∼76 μm and ∼51 μm are achieved in the new one. The relation between metal hole diameter and gain is measured in [20]. Gain of single GEM increases factor ∼1.5 by making the metal hole diameter smaller from 84 μm to 76 μm. Triple GEM is used in our measurement, so factor $1.5^3 \sim 3.4$ is expected as a gain difference due to the hole size. But 3.4 is too large for the measured difference. Above discussion is very premature and the measurements for the same setup should be done.

Though the effect of the hole size to gain is not made clear completely, gain of $\sim 10^4$ is achieved with large GEM by making hole size smaller and resolving flabbiness.

4 E16 simulation

Mass resolution of ϕ meson measurements is evaluated by Monte Carlo simulation. The main purpose of this simulation is to determine our experimental setup in detail.

4.1 Purposes

Purposes of the Monte Carlo simulation are followings,

1. To know the required position resolution of a GEM Tracker to achieve mass resolution of 5 MeV/c^2. Particularly,
   (a) When charged particles come in inclined to the GEM tracker in horizontal direction.
   (b) Minimum requirements in vertical direction.
2. Evaluate effects of several parameters on mass resolution.
   (a) Vertex position determination by thin target.
   (b) Magnetic field strength.

It is important to know 1.(a) to determine the configuration of a GEM tracker. Since there is a magnetic field in vertical direction, incident angle of charged particles to the GEM tracker becomes large in low momentum region. Readout configuration of the GEM tracker is anode strip and directly see the distribution of ionized electrons. Thus, spread of electrons due to inclined particles directly affect a position resolution of the tracker. Position resolution of inclined electron is strongly affected by measurement methods. The measurement methods are discussed in chapter 5 in detail. Thus, it is important to know the detailed relation between position resolution and mass resolution especially for inclined electrons.

Incident angle is defined as the angle between the track and horizontal(or vertical) axis. The definition of axis of beam line is shown in Fig. 24 and of GEM chamber is shown in Fig. 25. The horizontal(vertical) axis of GEM tracker depends on which detector segment we see. The amount of charge does not tell the position where inclined charged particle passed because the points where ionization occurs spread along the track. So to detect charged particle which encounter inclined to GEM tracker more precisely, other information is necessary, for example drift time of ionized electrons. Drift time is the time which is taken for the ionized electrons to reach the readout strips. The points of the ionization can be calculated by drift velocity and drift time and the track of an incident particle is reconstructed in a GEM chamber.

The configuration of the bottom side of readout strips is determined using a result of 1.(b). The bottom side strips measure the hit position in vertical direction. If the resolution in vertical direction need not to be as high as in horizontal, the strip pitch of the bottom side can be made coarser than the top side and the number of readout channels is decreased.

The required resolution for vertex position is derived in 2.(a) because it relates to the design of the target. If high resolution is necessary at for the vertex, the use of thin target such as wire target should be considered.

It is investigated whether mass resolution of 5 MeV/c^2 is achievable by making magnetic field stronger in 2.(b). Now 0.77[Tm] is considered as a limit of $\int BdL$.

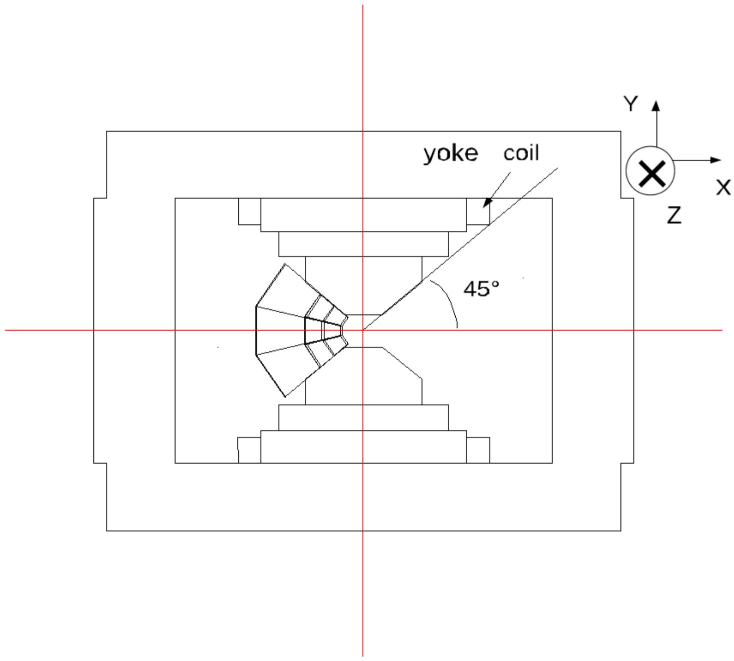

Figure 24: Front view of the magnet

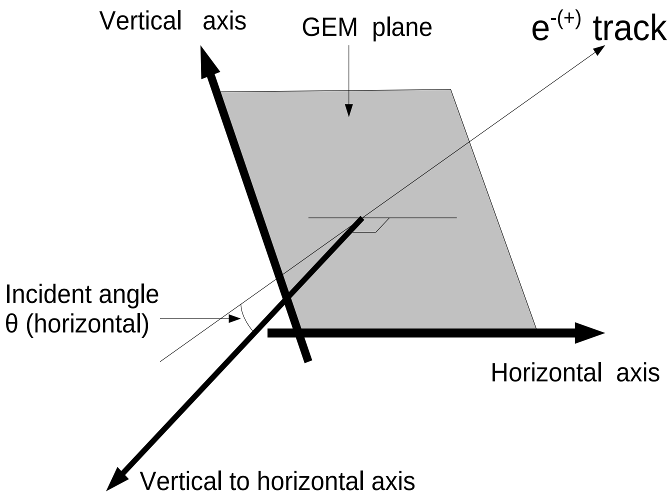

Figure 25: Definition of axis and incident angle in GEM chamber.

4.2 Procedure of simulation

The procedure of Monte Carlo simulation is as follows.

1. **Generation of ϕ meson**:

   Initial momentum of ϕ meson is generated by the nuclear cascade code JAM[21], in 30 GeV p + Cu reactions. JAM well reproduces the kinematical distributions of ϕ and ω mesons in 12 GeV p + C/Cu reactions[6].

   The mass of ϕ meson is generated by random number following Breit-Wigner distribution expressed as,

   $$BW(m) = \frac{\Gamma^2/4}{(m - m_0)^2 + \Gamma^2/4}$$

   Here, Γ is the width of ϕ and 4.26 MeV/c^2 is used. m_0 is the pole mass of ϕ and 1.019456 GeV/c^2 is used. $\beta\gamma$ and mass distribution of generated ϕ are shown in Fig. 26.

2. **Two body decay of ϕ**

   ϕ meson decays into e$^-$ and e$^+$. In the rest frame of ϕ, both e$^-$ and e$^+$ bring the energy of a half of the invariant mass of ϕ. A direction of

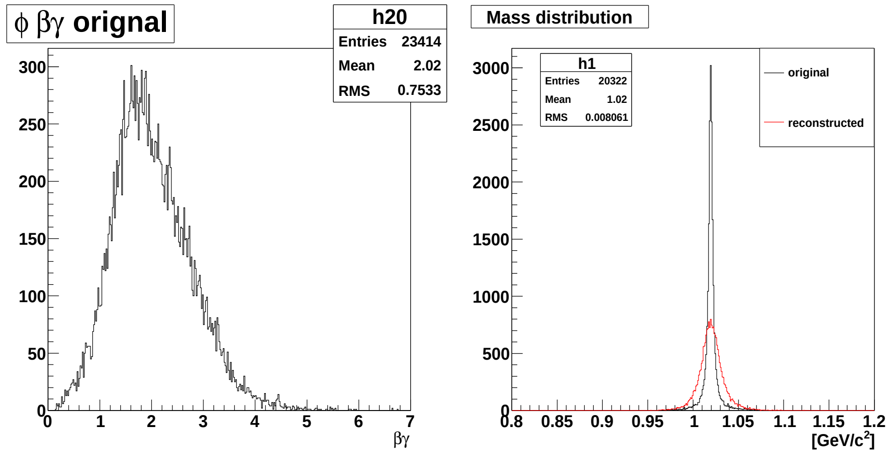

Figure 26: (left) $\beta\gamma$ distribution of simulated ϕ, (right) Typical mass distribution. Black line shows mass distribution of original ϕ. Red line is ϕ reconstructed by fitting the tracks of e^+e^-. Acceptance is taken into account in both figures.

momentum is determined by random numbers θ and ϕ in polar coordinates. Thus the momentum of either e^- or e^+ in the rest frame of ϕ is as following,

$$\begin{aligned} p_x &= \frac{M_\phi}{2} \sin\theta \cos\phi \\ p_y &= \frac{M_\phi}{2} \sin\theta \sin\phi \\ p_y &= \frac{M_\phi}{2} \cos\theta \end{aligned}$$

Direction of e^+ and e^- momentum are generated uniformly in 4π at the rest frame of ϕ. At last, e^- and e^+ are boosted to lab frame.

3. **Vertex position of e^+e^-**

A vertex position where ϕ decays is randomly generated. The distribution of vertex position is Gaussian in x and y direction(vertical to beam) and uniform in z direction. σ of the Gaussian in x and y direction are fixed to 900 μm. The distribution of vertex position is shown in Fig. 27. This is considered as the size of achieved beam spot. Vertex is dispersed uniformly over 100 μm in z direction which corresponds to a target thickness.

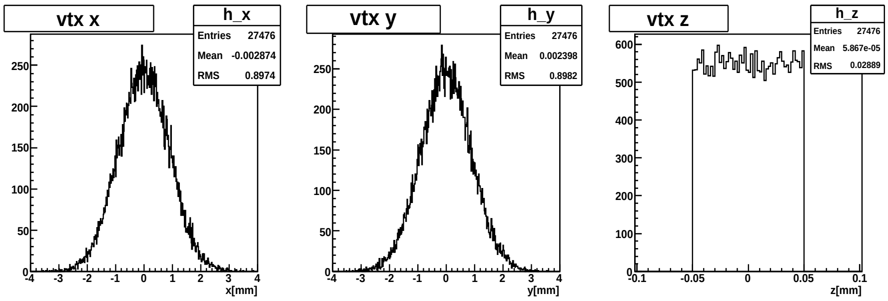

Figure 27: Vertex position distribution. (left) x direction, (middle) y direction, (right) z direction.

4. **Generation of e^+ and e^- tracks and hit positions**

   Then e^+ and e^- are transported in a magnetic field. Transportation is done by the fourth-order Runge-Kutta method. Multiple scattering by air and detector component is taken into account. The displacements of hit positions and momentum direction are added at the planes of GEM chambers. Schematic view of the transportation is shown in Fig. 28.

   The effects of multiple scattering are calculated based on the radiation length of each component. Radiation length of a GEM chamber is estimated ~0.3% as described in Table. 3 of chapter 3. The deflection angle by multiple scattering is assumed to follow Gaussian whose width is θ_0 expressed below[25]. p is the momentum of electron and X_0 is the radiation length of the scattering material. Radiation length(X_0) of air is 36.66 [g/cm^2] and x/X_0 is calculated from the density 1.2931 [g/l](STP) and the track length. y_{plane} and θ_{plane} are the displacements of the hit position and momentum direction by multiple scattering as shown in Fig. 28.

$$\begin{aligned}
\theta_0 &= \frac{13.6MeV}{\beta cp}\sqrt{\frac{x}{X_0}}[1 + 0.038\ln(\frac{x}{X_0})] \\
y_{plane} &= z_1\frac{x\theta_0}{\sqrt{12}} + z_2\frac{x\theta_0}{2} \\
\theta_{plane} &= z_2\theta_0
\end{aligned}$$

Here z1 and z2 are independent Gaussian random numbers whose mean is 0 and σ is 1. The hit position and particle direction are smeared according to above calculation when a particle hits the GEM plane. Hit position is additionally smeared by the position resolution of GEM tracker.

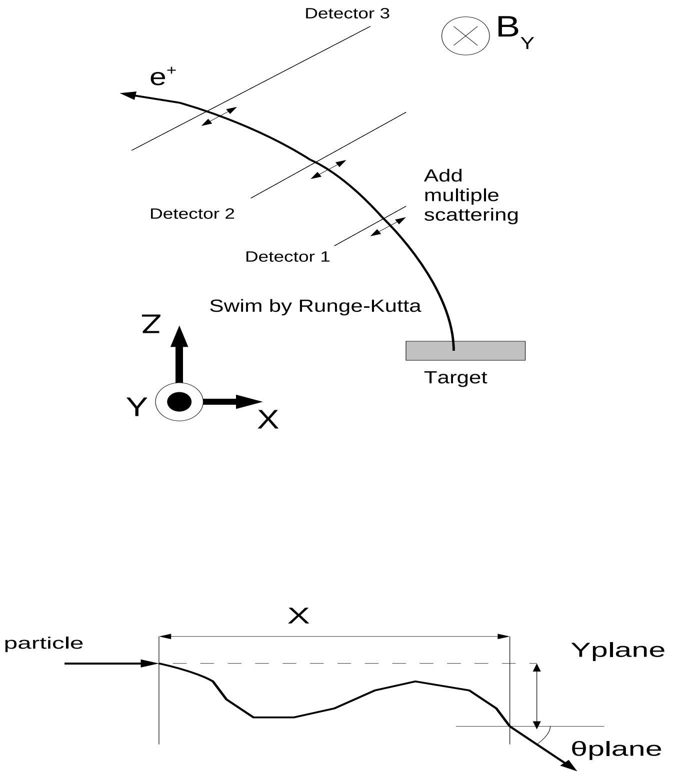

Figure 28: (top) Schematic view of transportation of electron. (bottom) Variables in the calculation of multiple scattering[25].

5. **Momentum reconstruction**

Momentum of e$^+$ and e$^-$ are reconstructed by the simultaneous fit of the two tracks with a common decay vertex. Fit parameters are the vertex position: (vx, vy, vz) and momentum vector of e$^+$ and e$^-$ at the vertex: (px_e$^+$, px_e$^+$, px_e$^+$) and (px_e$^-$, px_e$^-$, px_e$^-$).

Fit is performed to minimize χ^2 which is defined as,

$$\chi^2 \quad = \sum_{i=x,y,z} \left(\frac{vtx\_fit_i - vtx\_org_i}{\sigma^i_{vtx}}\right)^2$$

$$+ \sum_{j=e^-,e^+,k=1,2,3,l=h,v} \left(\frac{fit\_position_{jkl} - det\_position_{jkl}}{\sigma^l_{det}}\right)^2$$

Where *vtx_fit* is a vertex position as a fit parameter, *vtx_org* is a reference point of the vertex, *fit_position* is a track-hit position on each GEM chamber determined by the fit, and *det_position* is a simulated (detected) hit position on the GEM chamber. σ_{vtx} is the resolution of vertex determination and σ_{det} is the position resolution of GEM chamber. k denotes the detector number. The inner GEM (100×100 mm^2) is '1', the middle one (200×200 mm^2) is '2' and the outer one is '3' (300×300 mm^2). l denotes the direction of readout strips, *horizontal* or *vertical*.

Two assumptions are put in the simulation procedure. First, the vertex position of e$^-$ and e$^+$ is common. Second, we know the target position where ϕ decayed when fit the tracks.

4.3 Mass resolution as a function of position resolution

Mass resolution is evaluated by simulation changing the position resolution of GEM. The goal of mass resolution is 5 Mev/c^2. The double peak of ϕ is expected to be observed with the resolution of 5 MeV/c^2.

4.3.1 inclined electrons

GEM tracker consists of three GEM chambers which line in radius direction. Each size is 100×100 mm^2, 200×200 mm^2 and 300×300 mm^2. They are put at 20 cm, 40 cm and 60 cm away from the target.

Mass resolution is estimated changing the position resolution of each chamber according to the incident angle. The fraction of inclined electrons for each chamber is in Table. 9 and the correlation of incident angle of e$^-$ and e$^+$ is in Fig. 29. More than ∼80% electrons encounter the chamber within 15° and there is a strong correlation that both e$^+$e$^-$ come within 15°. So the position resolution up to 15° is expected to be important.

Three sets of the position resolution according to incident angles in horizontal direction are examined to check the dependency. They are described in Table. 11. The resolution is changed linearly above 15° but fixed to 100 μm from 0 to 15° in "case1". This case is based on a result of a test experiment for the resolution of GEM tracker[22]. The measured position resolution is shown in Table. 10. The second case "case2" changes resolution linearly above 0° but fixed to 100 μm for 0°. In the "case3", the resolution

	horizontal or vertical	0-15°	15-30°	30° <
detector1	h	95%	5%	<1%
detector2	h	85%	15%	<1%
detector3	h	78%	21%	<2%
detector1	v	99%	<1%	0%
detector2	v	99%	<1%	0%
detector3	v	99%	<1%	0%

Table 9: The fraction of inclined electrons. Detector1 corresponds to the inner chamber, 100×100 mm^2 GEM. Detector2 is the middle, 200×200 mm^2. Detector3 is the outer, 300×300 mm^2.

for 15°∼30° is fixed to 500 μm, but changed for 0° ∼ 15° (Table. 12). Case3 is used to see the effect of the position resolution for 0°∼15° incident angle to the mass resolution.

Fig. 30 shows the dependence of mass resolution on position resolution of case1 and case2. Mass resolution degrades less than 10% in case1, but degrades ∼30% in case2 according to the position resolution for 30°.

A plot of electron momentum dependence of $\Delta p/p$ is shown in Fig. 31. $\Delta p/p$ and p have a relation as following.

$$\frac{\Delta p}{p} = \frac{8\Delta S}{0.3(\int BdL)L} \cdot p$$

Here S[m] is sagitta and B[T] is the magnetic field in y direction. L[m] is the length of a track in magnetic field. So $\Delta p/p$ is proportional to p if position resolution of a detector is more dominant than the multiple scattering effect. Δp is derived as the width of $|p_{fit}| - |p_{org}|$ distribution fitted with gaussian. $|p_{fit}|$ is the magnitude of the momentum calculated by fitting the track. $|p_{org}|$ is the generated momentum by two body decay of ϕ meson. The degradation of momentum resolution according to the position resolution is seen in Fig. 31.

Fig. 32 is the result of case3 and mass resolution degrades.

These results show that the resolution for 30° inclined electrons is not important because mass resolution degrades in case3 but not in case1. The deterioration of the position resolution for 0°∼15° directly leads to the deterioration of mass resolution.

	0°	15°	30°
resolution [μm]	70	100	140

Table 10: Measured position resolution of GEM

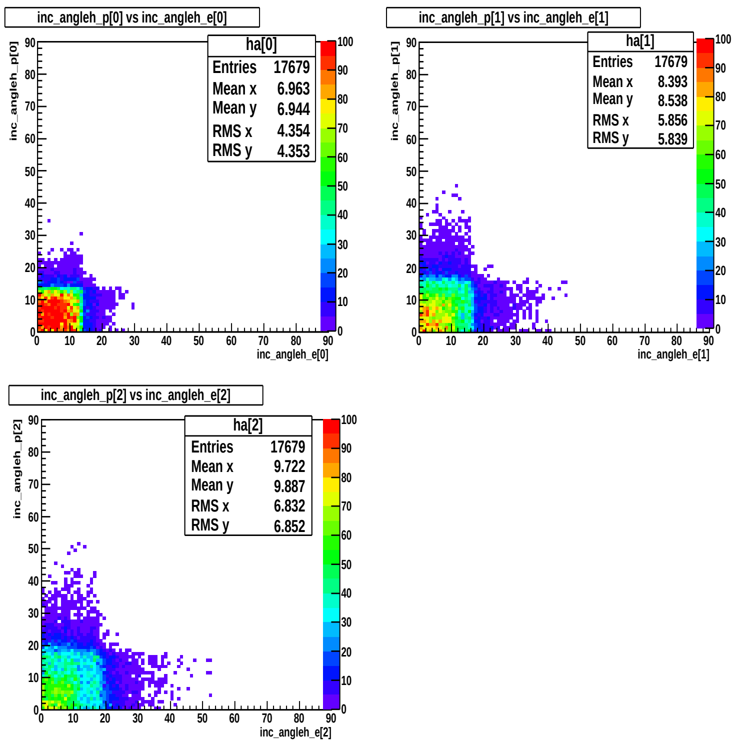

Figure 29: Correlation of the incident angles of e^+e^-. (top left) The correlation of incident angles in the most forward chamber(100×100 mm^2 GEM). (top right) In the middle chamber (200×200 mm^2 GEM), (bottom left) In the most rear chamber (300×300 mm^2 GEM).

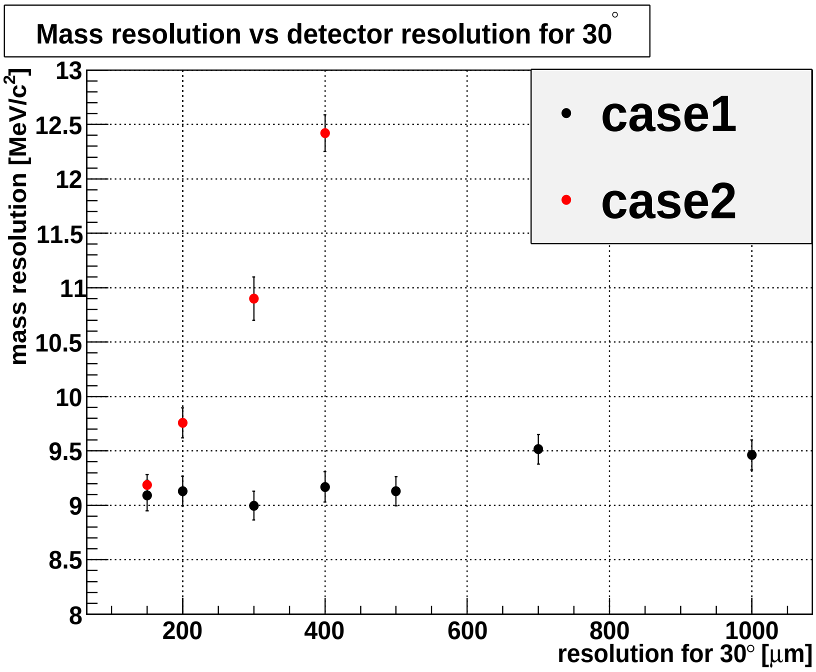

Figure 30: Mass resolution vs position resolution at 30°

	position resolution [μm]										
incident angle [°]	case1(Black)							case2(Red)			
0	100	100	100	100	100	100	100	100	100	100	100
15	100	100	100	100	100	100	100	125	150	200	250
30	150	200	300	400	500	700	1000	150	200	300	400

Table 11: Sets of position resolutions simulated.

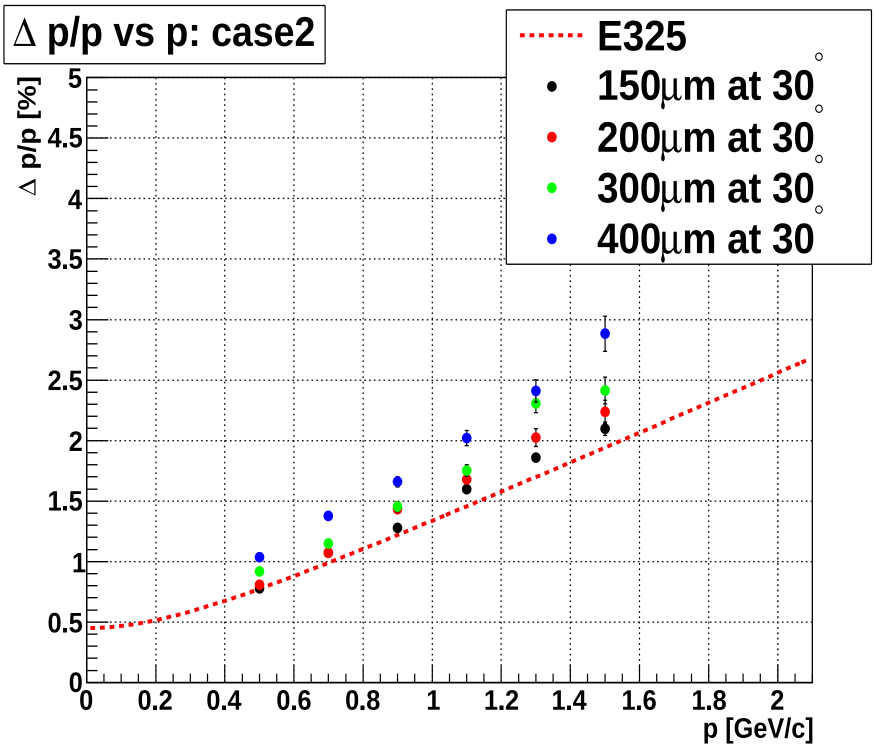

Figure 31: Δp/p vs p of case2. $(\sigma^x_{vtx},\ \sigma^y_{vtx},\ \sigma^z_{vtx})$=(0.9, 0.9, 0.05) [mm], vtx_org=(0,0,0).

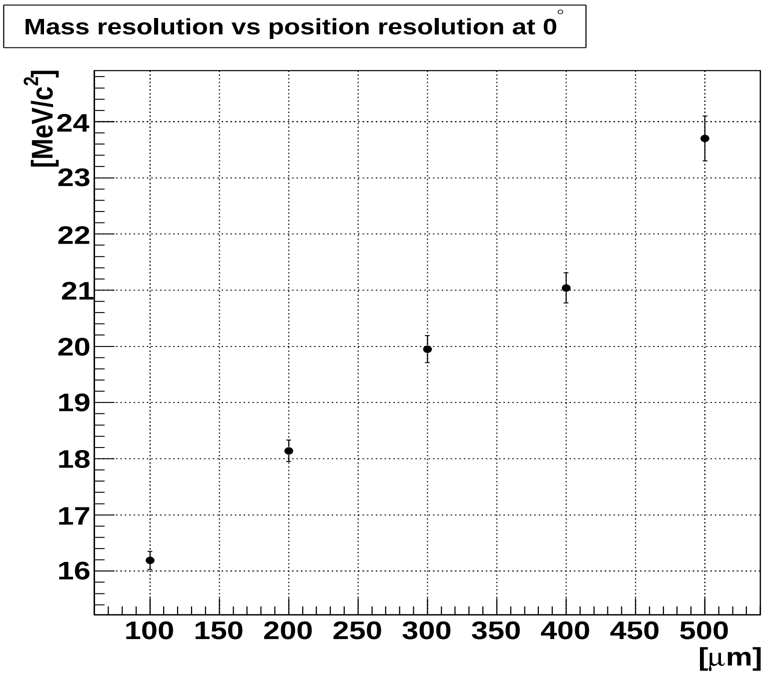

Figure 32: Mass resolution vs position resolution at 0° of case3.

incident angle[°]	case3 position resolution [μm]				
0	100	200	300	400	500
15	500	500	500	500	500
30	500	500	500	500	500

Table 12: The resolution setup of case3.

4.3.2 Vertical position resolution

The dependence of mass resolution on the position resolution in vertical direction is also evaluated.

The hit position in vertical direction is used to derive the momentum in y direction, P_y. P_y is generally smaller than $P_T (= \sqrt{P_x^2 + P_z^2})$ as shown in Fig. 33. So the vertical position resolution is expected to be less effective to mass resolution than horizontal direction.

The mass resolution is evaluated with the vertical position resolution which is constant according to the incident angle, since more than 99% of electrons come within 15° (Table. 9). Result is shown in Fig. 34.

Even if the vertical resolution was 1 mm, the mass resolution degrades less than 4.5% compared to 200 μm.

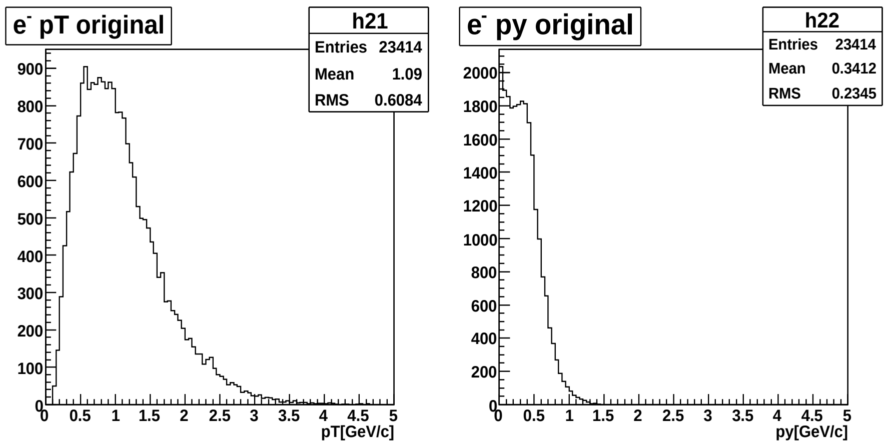

Figure 33: P_T and P_y of e^-. These momentum are original but not derived from fitting.

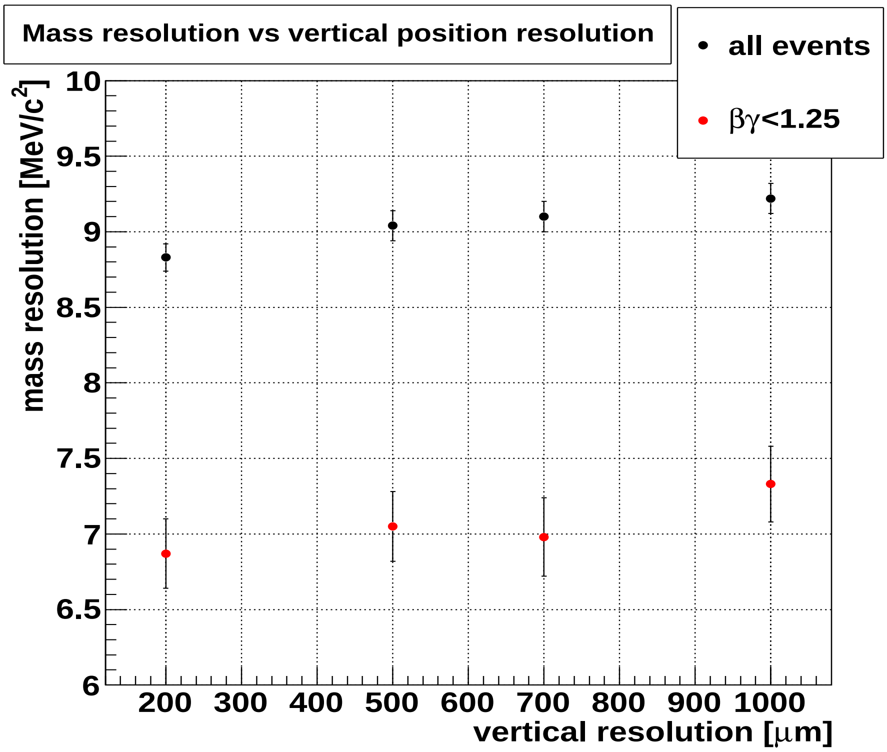

Figure 34: Mass resolution vs position resolution in vertical direction. (σ^x_{vtx}, σ^y_{vtx}, σ^z_{vtx})=(0.9, 0.9, 0.05) [mm], vtx_org=(0,0,0) and horizontal resolution of detector for 0°, 15° and 30° are 100, 100 and 150 μm.

4.4 Other parameter dependence

4.4.1 Vertex reconstruction

The real vertex position is unknown in the experiment, so the vertex position is reconstructed with the resolution of vertex position. The effect of the vertex position resolution to the mass resolution is evaluated.

Track is fitted by calculating χ^2 on the target, the inner, the middle and the outer GEM chambers. So the vertex position has to be assumed as somewhere on the target to calculate χ^2 since there is no detector for the vertex position. Two cases are investigated.

1. Position of the real vertex is known with some resolution.

   vtx_org_i is set as the position of the generated vertex in calculating χ^2 and the resolution of the vertex σ_{vtx} is changed. The results of

   $(\sigma^x_{vtx}, \sigma^y_{vtx}, \sigma^z_{vtx})$=(0.9, 0.9, 0.05), (0.5, 0.5, 0.05), (0.1, 0.1, 0.05) [mm]

   are compared.

2. Position of real vertex is unknown and the center of the target is used in χ^2 calculation.

   $(vtx\_org_x, vtx\_org_y, vtx\_org_z)$=(0, 0, 0) and

   $(\sigma^x_{vtx}, \sigma^y_{vtx}, \sigma^z_{vtx})$=(0.9, 0.9, 0.05) [mm]

   are assigned in χ^2 calculation. σ_{vtx} is determined by the size of beam.

A plot of $\Delta p/p$ is shown in Fig.35.

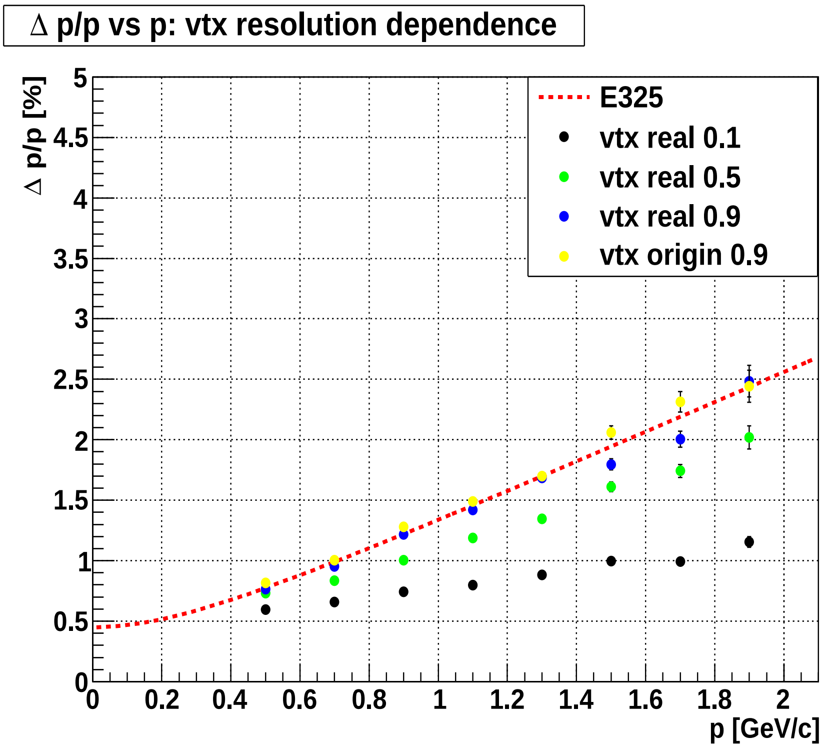

Figure 35: Δp/p vs p: vertex resolution dependence. 100, 100 and 150 μm are assumed for 0°, 15° and 30° incident angle as horizontal position resolution.

The mass resolution is shown in Fig. 36. X axis in Fig. 36 is $\sigma_{vtx}^{x(y)}$ [mm]. Mass resolution of 5.1 MeV/c^2 is achieved with the vertex resolution of 100 μm. The use of wire target or narrowing beam spot is considered as a way to achieve high vertex resolution.

4.4.2 Magnetic field

Mass resolution of 5.1 MeV/c^2 is achieved with the position resolution of 100 μm, 100 μm and 150 μm for 0°, 15° and 30° and vertex resolution of 100 μm. $\int BdL$ has been 0.73 [Tm] in the above simulation and the mass resolution is evaluated with a stronger magnetic field.

The configuration of magnet is determined by the detector acceptance as shown in Fig. 24. The tracker and HBD are designed to cover ±45° vertically. So to keep the acceptance, current is increased in the coil to strengthen the magnetic field without narrowing the gap between the pole pieces. The field is calculated by POISSON which is a package to calculate

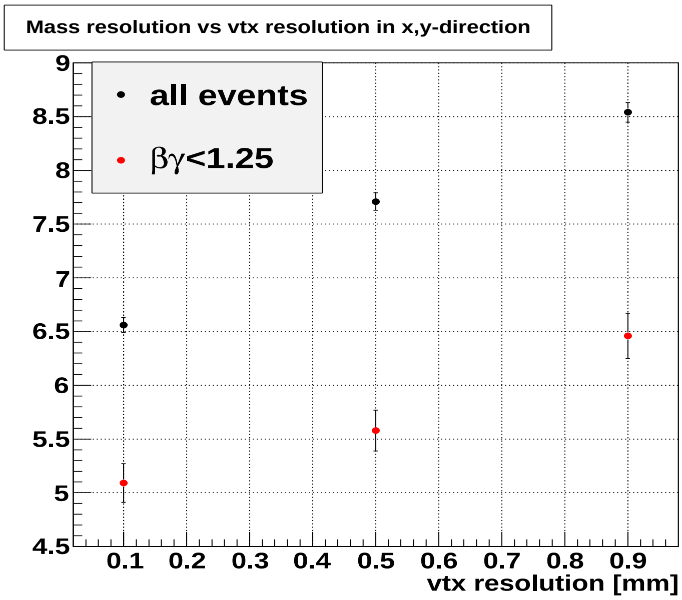

Figure 36: Mass resolution: vertex resolution dependence. The horizontal resolution for electrons is 100, 150 and 200 μm for 0°, 15° and 30°.

a magnetic field symmetric around y axis. 1/4 of the magnet and a result of POISSON is shown in Fig. 37. The current in the coil is changed to evaluate the dependence of mass resolution on the magnetic field. The current and $\int BdL$ are shown in Table. 13. $\int BdL$ is calculated about y component of magnetic field up to 600 mm from the target in radial direction. The B_y [T] and $\int BdL$ [Tm] at R [m] in radius are shown in Fig. 38. The difference among the configurations of more than 2000A is smaller than between 2000A and 1500A because of the saturation of iron's magnetization.

Mass resolution of 4.6 MeV/c^2 is achieved with 2500A, $\int BdL = 0.77$ [Tm]. Mass resolution is improved more at 3000A, but it is difficult to use such high current due to the inadequacy of power supply. So 2500A is necessary to achieve better than 5 MeV/c^2 mass resolution.

$\Delta p/p$ plot and mass resolution for each $\int BdL$ are shown in Fig. 39 and 40.

	1560A	2000A	2500A	3000A
[Tm]	0.64	0.73	0.77	0.80

Table 13: $\int$BdL(integral 60cm from the target)

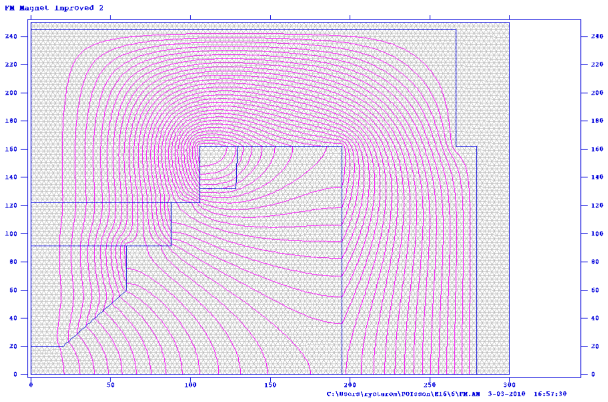

Figure 37: Field map calculated by POISSON. 1/4 of the magnet is shown.

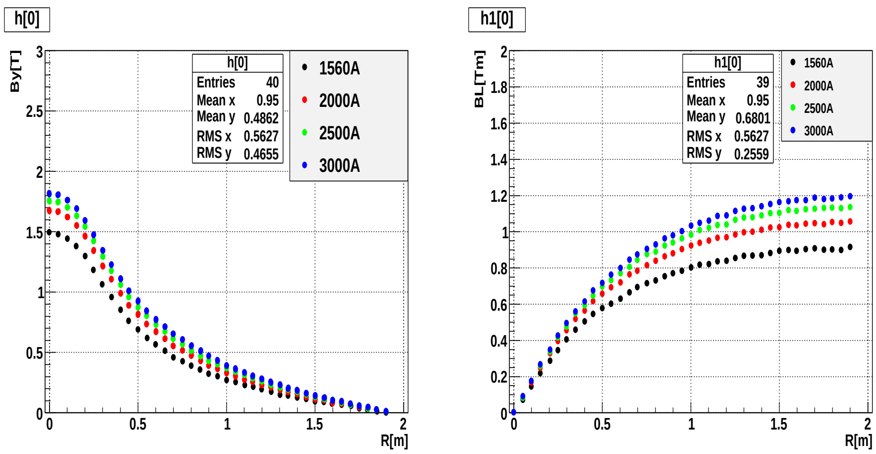

Figure 38: (left) By[T] vs radius[m] for each setup of current., (right) $\int$BdL[Tm] vs radius[m].

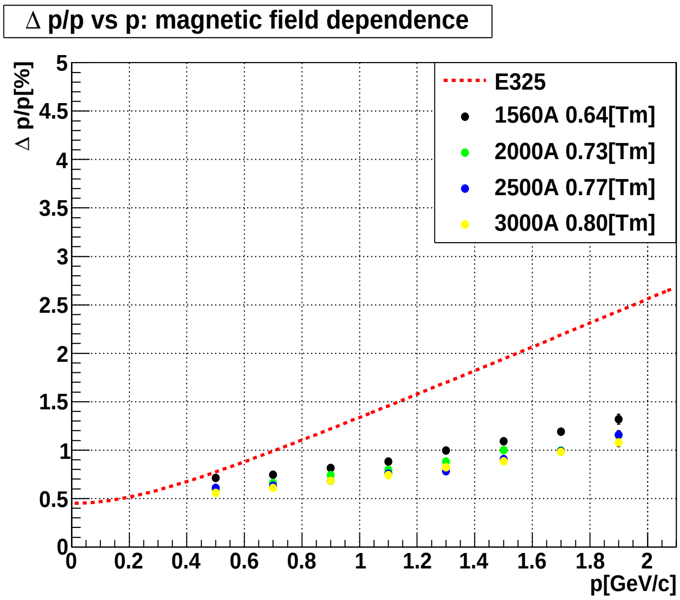

Figure 39: Δ p/p vs p: magnetic field dependence. (σ^x_{vtx}, σ^y_{vtx}, σ^z_{vtx})=(0.1, 0.1, 0.05)[mm], vtx_org is generated vertex position, and σ_{det} is 100, 100 and 150 μm for 0°, 15° and 30°.

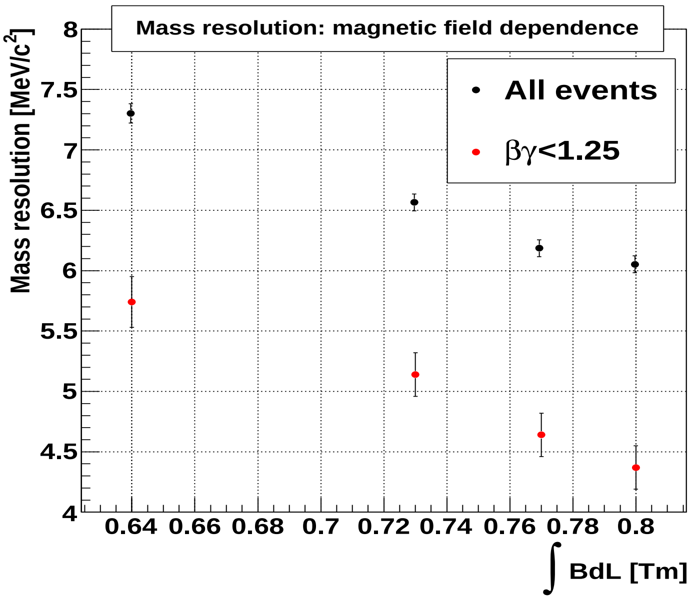

Figure 40: mass resolution:magnetic field dependence

4.5 Conclusion

The results with parameters are shown in Table. 14.

The horizontal position resolution of 100 μm up to 15° is necessary. This is related to the strip pitch of the readout. The relation between strip pitch and position resolution is studied by the beamtest and discussed in chapter 5.

The position resolution of vertex is also effective to mass resolution. If the resolution of 100 μm was achieved, mass resolution is improved by $\sim$2 MeV/c^2 compared to using only beam size information about vertex postition. Wire target is considered as a candidate for the resolution of 100 μm . Of course magnetic field improves the mass resolution and 5 MeV/c^2 is achieved by 0.77 Tm. 0.80 Tm is available if 3000A was added to coil, but it is difficult due to the facility.

position resolution horizontal[μm]	$0\circ$	100	100	100
	15°	100	100	100
	30°	150	150	150
position resolution vertical [μm]		200	200	200
vertex resolution	reference for χ^2	center of target	real	real
	resolution[μm]	900	100	100
$\int BdL$(up to 600mm from target)[Tm]		0.73	0.73	0.77
mass resolution [MeV/c^2]	all	8.8	6.6	6.2
	$\beta\gamma(\phi) < 1.25$	6.9	5.1	**4.6**

Table 14: Parameters and mass resolution.

5 Beamtest

We performed a beamtest to evaluate an efficiency and a position resolution of GEM tracker. The test is done with momentum of 750 MeV/c positron beam at LNS, Tohoku University.

5.1 Purposes

Purposes of the beamtest are following,

1. To operate large GEM tracker, such as 200×200 mm^2 and 300×300 mm^2 GEM and evaluate their position resolution.

   100×100 mm^2 GEM is operated stably and achieved 100 μm position resolution in the our previous research [22]. The next step is to test a position resolution with large size GEM. The stability of large GEM also should be tested because it is expected to have higher probability to spark than 100×100 mm^2 GEM. In addition, there are difficulties to manufacture large GEM precisely, so the full operation and beam test of large GEM are important.

2. To evaluate the position resolution in vertical direction.

   The position resolution in vertical direction needs to be evaluated. In the previous research, performance of horizontal direction is mainly studied. The signal charge is expected to be smaller than horizontal strips because vertical strips are placed on the bottom side of the readout foil. So the efficiency and position resolution in vertical direction should be studied carefully.

   Also, in offline analysis, position resolution with wider strip pitch are evaluated, since our simulation shows that position resolution is less needed in vertical direction and the number of readout channels can be reduced if strip pitch becomes wider. For this purpose, signal charges of neighborhood strips are merged and position resolution is evaluated with wider strip pitch.

3. To evaluate the position resolution without waveform information.

   The waveforms of signals are taken by FADC in the beamtest, however the form of data changes according to the readout electronics in the real experiment. If only hit strips and timing information are derived by comparator as front-end electronics, the waveforms are unknown. As a result, the ADC value and the position of the peak of signal are unknown. So the position resolution is evaluated using following information only.

- Hit strip information: A threshold for ADC value is set and the strips which exceed the threshold are defined as hit strips. The threshold is common for all the strips.
- Timing information: The timing at which the strip exceeds the threshold is derived by the clocks of FADC.

5.2 Beam line

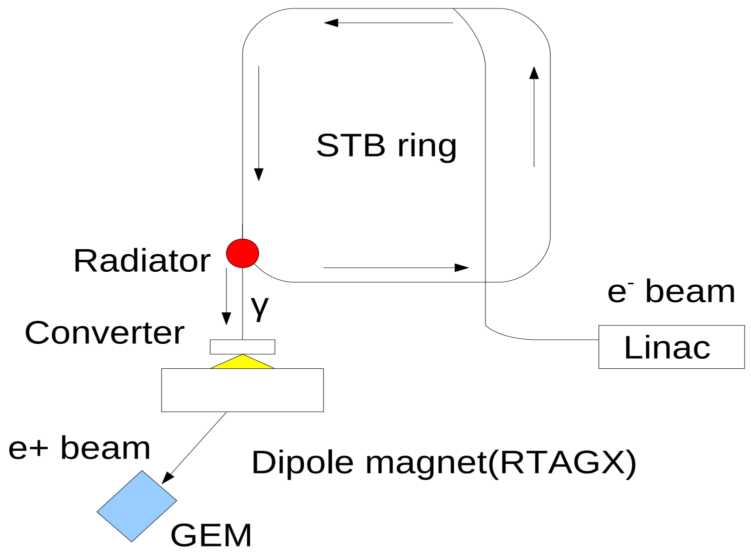

Figure 41: Schematic view of the beamline.

The test experiment is done with positron beam at the GeV-γ beamline of Laboratory of Nuclear Science, Tohoku University. The beam property is shown in Table. 15. Pulse beam of electron is accelerated up to 200 MeV/c^2 and sent to the STB ring. Then STB ring stretches and boosts the beam up to $\sim$1.2 GeV/c^2. γ ray is emitted by the bremsstrahlung of electron beam in STB ring. Carbon fiber is used as a radiator and high energy γ ray is emitted when e^- crosses the radiator[23]. At last positron beam is generated by the pair creation of γ ray at the converter (Fig. 41). The energy of e^+ beam can be selected by the current of dipole magnet ($RTAGX$). Momentum of 750MeV/c beam is used in the beamtest.

particle	momentum	size(diameter)	rate	duty factor
e^+	750MeV/c	5cm	$\sim$100Hz/cm^2	0.5

Table 15: Beam property.

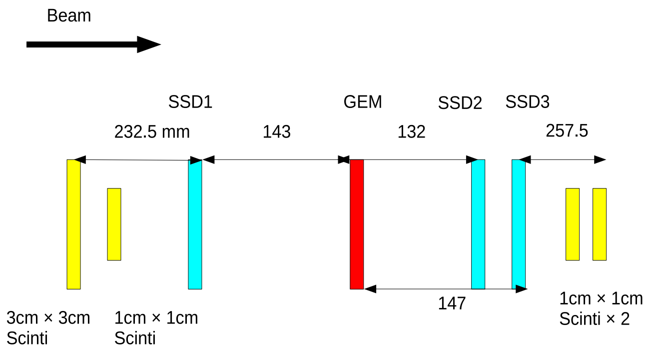

Figure 42: The setup of beamtest

5.3 Test setup

Schematic view of the setup is shown in Fig. 42. Trigger is made by a coincidence of 4 scintillators. The sizes of the scintillators are 3×3 cm^2, 1×1 cm^2, 1×1 cm^2, and 1×1 cm^2 from the upper stream. The readout region of GEM is 1.1 cm×1.1 cm^2 for 350 μm pitch readout and 2.2 cm×2.2 cm^2 for 700 μm pitch readout, respectively. The readout region is determined by a limitation of the number of channels of FADC, though GEM and readout foil itself have the size of 100×100 mm^2, 200×200 mm^2 or 300×300 mm^2. 32 channels are connected to FADC and each waveform is sampled at 100 MHz by FADC. The input range of FADC is 0$\sim$-1V and resolution is 8bit. The time range of FADC is $\sim$6 μs and this is longer than the time constant of signal amplifier, 1 μs. GEM signals are delayed $\sim$115 ns to match the trigger decision timing. The angle between a GEM chamber and beam is changed by inclining GEM chamber on the table. Tested angles are 0°, 15° and 30°.

As a reference for the hit position, three Silicon Strip Detectors (SSDs) are also installed. Each SSD gives the hit position in horizontal direction. SSD's strip pitch is 80 μm and has 384 readout strips. So the sensitive area of SSD is $\sim 3\times 3$ cm^2. Residual is calculated as the difference between the hit position in GEM and the position interpolated by the hit positions of SSDs.

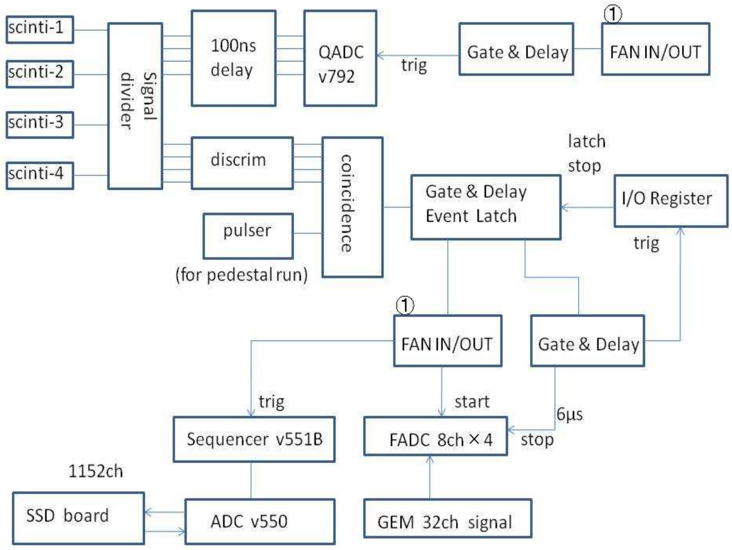

Figure 43: The DAQ system

5.4 Analysis procedure

5.4.1 SSD analysis

Offset and common noise subtraction

The offset of ADC is subtracted using clock trigger (pedestal) data. Clock trigger data contains the ADC values of 1152ch without beam.

In addition, common mode noise is evaluated and subtracted event by event.

1. Offset subtraction: Offset for each channel is estimated with clock trigger data. First, common noise in the clock trigger data is evaluated before the offset evaluation because common noise changes event by event.

SSDs have common mode noise in every 128ch due to VA-chip characteristic. So common mode noise is calculated as following.

$$n_i = \sum_{j=1}^{128} \frac{Q_{ij}}{128} \quad (i = 1, 2 \ldots 9)$$

n_i is the common noise of i th VA-chip. Q_{ij} is the ADC value of j th strip in i th VA-chip. n_i is calculated event by event.

Then common noise is subtracted from each strip's ADC value. The offset is the average of $Q_j - n_k$ for whole events.

$$X_i = \sum_{evt=1}^{N} \frac{Q_{i\ evt} - n_k}{N} \quad (i = 1, 2 \ldots 1152, k = 1, 2 \ldots 9)$$

Here X_i is the offset of i th strip. N is the number of events and k is the VA-chip number. The X_i is subtracted as a pedestal for each channel.

2. Common mode noise subtraction: Common mode noise are subtracted from the data with beam. Common mode noise is calculated as the average of ADC values of every 128ch event by event. So corrected ADC value for each SSD strip is as following.

$$Q_{cor\ i} = Q_i - X_i - n_j \quad (i = 1, 2 \ldots 1152, j = 1, 2 \ldots 9)$$

The process of the subtraction of common noise and offset is shown in Fig. 44.

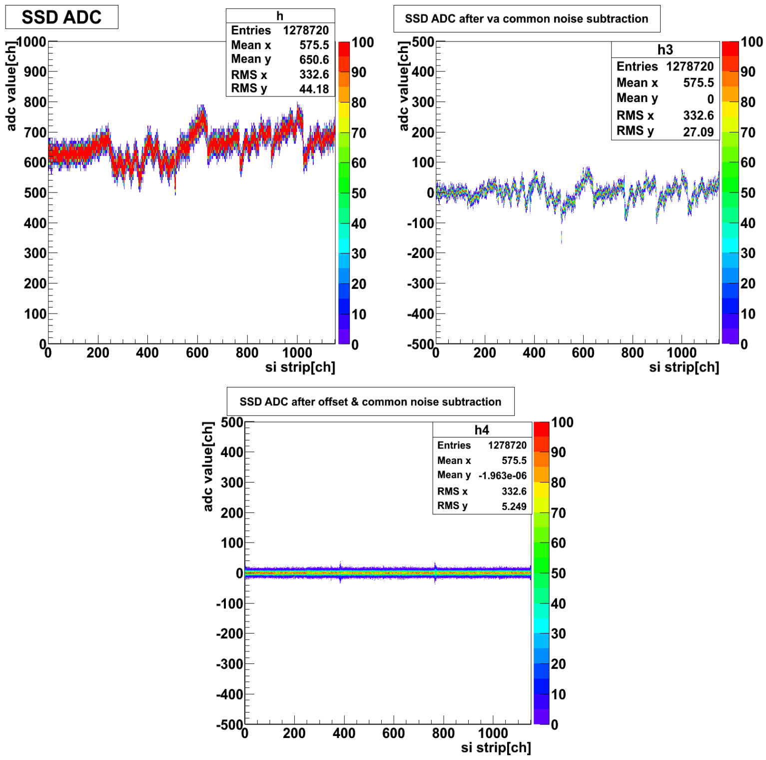

Figure 44: (top left) ADC value vs SSD ch before offset & common noise subtraction, (top right) After the subtraction of VA-chip common noise, (bottom) After the subtraction of offset for each channel.

SSD hit reconstruction

To select valid events for SSDs, significance is defined as following.

$$S_i = \frac{Q_{corri}}{\sigma_i} \quad (i = 1, 2 \ldots 1152)$$

S_i is the significance of i th strip. σ_i is the RMS of ADC distribution derived from clock trigger data. A significance distribution for one SSD strip is shown in Fig. 45. Valid strips are defined as $S_i \geq 5$.

The hit position of each SSD is calculated by weighted mean method. It is expressed as,

$$x_i = 80[\mu m] \times \frac{1}{\sum_{j=1}^{N} S_{a_j}} \sum_{k=1}^{N} a_k \times S_{a_k} \quad (i = 1, 2, 3)$$

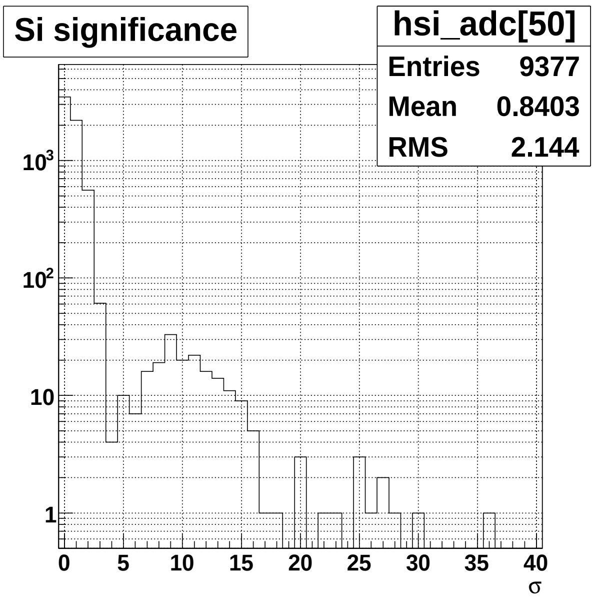

Figure 45: Significance distribution of one SSD strip.

N is the number of strips which are $S_i \geq 5$ and a_k is the strip number. 80 μm is the strip pitch. Hit position is calculated as the weighted mean of S_i.

Event Cut

Event selection is done by SSD information.

- **Hit requirement for 3 SSDs**

  The number of strips which satisfy $S \geq 5$ is called "n_hit_i". i denotes the SSD number 1, 2 or 3. The hit requirement for three SSDs is expressed as following.

  $$(n\_hit_1 > 0) \cap (n\_hit_2 > 0) \cap (n\_hit_3 > 0)$$

  All layers of SSDs are required to have hits.

- **Double hit cut**

  In addition, double track rejection is applied. If an event includes a strip a_{strip} which satisfies following conditions, such event is rejected.

  1. $a_1 < a_{strip} < a_{n\_hit}$
  2. $S_{a_{strip}} < 5$

$$1. \cap 2.$$

a_i is strip number and i is the hit strip number. n_hit is the number of hit strips of one SSD. For example, if No.1, 2 and 4 are the strips whose significance are over 5, $n\_hit = 3$ and $a_1 = 1$, $a_2 = 2$, $a_3 = 4$. Since $a_1 = 1 < a_{strip} = 3 < a_3 = 4$ and $S_3 < 5$, such event is rejected as a double hit event.

Interpolation of hit points

Hit position of GEM as a reference is calculated by the SSD's hit positions. The position along beam axis is determined geometrically and the track is assumed as a linear function $x = a \times z + b$ (Fig. 46). In the following analysis, SSD1 and SSD2 are used to interpolate the hit points, because the hit position of SSD3 is affected by the multiple scattering of SSD2 and worsens the residual distribution(Fig. 47). Parameters a and b are expressed as,

$$\begin{aligned} a &= \frac{x_1 - x_2}{z_1 - z_2} \\ b &= \frac{x_2 z_1 - x_1 z_2}{z_1 - z_2} \end{aligned}$$

Here x_1, x_2 and z_1, z_2 are the coordinates of hit positions of SSD1 and 2. Then the interpolated hit position by SSD (x_{SSD}) is calculated as an intersection point of a track and GEM plane as follows.

$$
\begin{aligned}
x &= a \times z + b \cdots formula\ of\ a\ track. \\
z &= gem\ position \cdots formula\ of\ GEM\ plane.\ (\theta = 0^\circ) \\
x &= \tan(\pi/2 + \theta)(z - gem\ position) \cdots formula\ of\ GEM\ plane.\ (\theta = 15^\circ\ or\ 30^\circ)
\end{aligned}
$$

Here θ is the incident angle of beam and *gem position* is the z coordinate of GEM plane. *gem position* is input by hand. The x coordinate of the intersection point x'_{SSD} is as following.

$$
\begin{aligned}
x'_{SSD} &= a \times gem\ position + b \cdots (\theta = 0) \\
x'_{SSD} &= \frac{gem\ position + b}{\tan(\pi/2 + \theta) - a} \cdots (\theta = 15^\circ\ or\ 30^\circ)
\end{aligned}
$$

Then, the hit position interpolated by SSDs x_{SSD} is calculated as following.

$$
x_{SSD} = \frac{x'_{SSD}}{\cos\theta}
$$

Schemateics of the interpolation is shown in Fig. 46

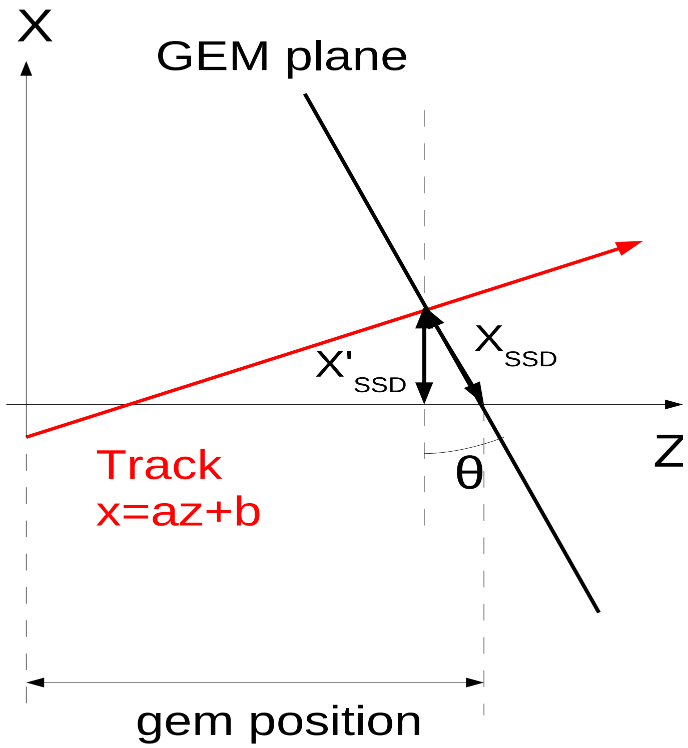

Figure 46: Schematic view of interpolation of SSD hit points.

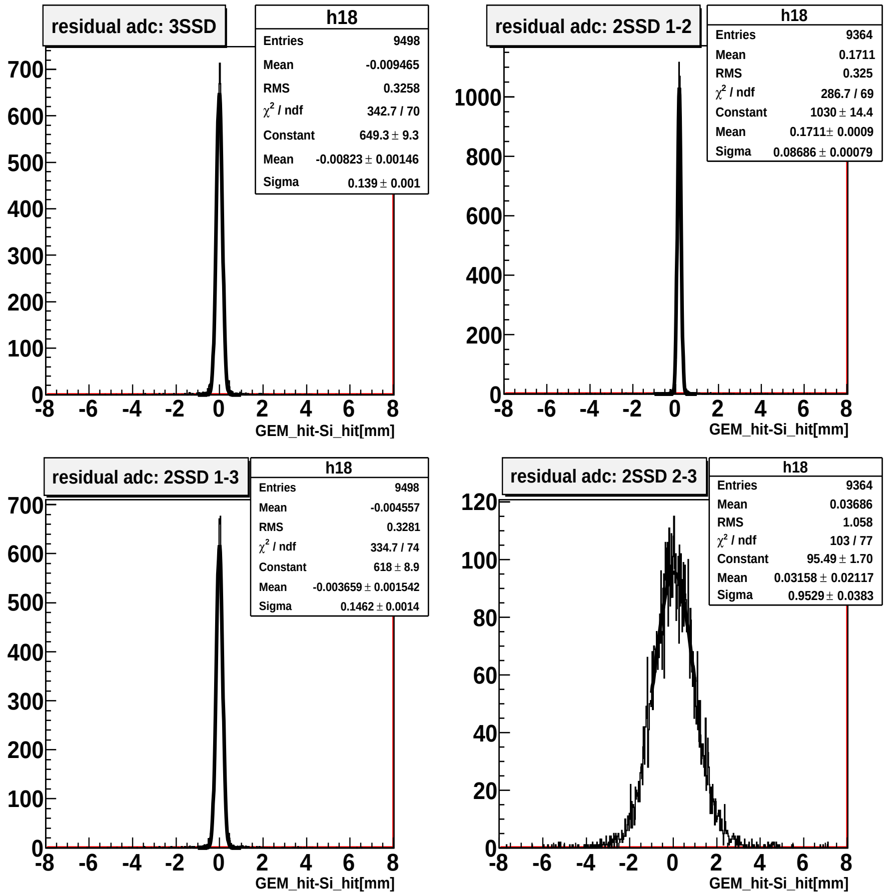

Figure 47: Residual distribution according to SSDs used for interpolation. (top left) All 3 SSDs are used. (top right) SSD1 & 2 are used. (bottom left) SSD1 & 3 are used. (bottom right) SSD2 & 3 are used. Using SSD1 & 2 achieves the best residual.

5.4.2 GEM analysis

Offset subtraction

Offset of FADC is calculated with the data of clock trigger run. The ADC data is taken for 640 clocks/event. The offset is calculated as a mean of ADC values for 640 clocks and all events as following,

$$X_i = \frac{\sum_{j=1}^{N} \sum_{k=1}^{640} Q_{ijk}}{N \times 640} \quad (i = 1, 2 \ldots 32)$$

X_i is the offset value of i th strip. N is the total number of events and k denotes the clock number. X_i is used to derive the corrected value of FADC in the data of runs with beam.

$$Q_{ij}^{corr} = Q_{ij} - X_i \quad (i = 1, 2 \ldots 32, j = 1, 2 \ldots 640)$$

Peak value of each FADC channel and finding max ADC strip

The peak value is obtained from each waveform. Peak value is the largest ADC value among 200 clocks from the trigger. 200 clocks correspond to 2 μs. This time range is determined by considering drift time from drift gap to the readout. The length from cathode to readout is $6+2+2+2 = 12$ [mm], so it takes 800 ns for electrons to reach the readout if the drift velocity is about 1.5 cm/μs. 1.5cm/μs is estimated by Magboltz [24] which calculates the drift velocity and diffusion constants of electrons in gas (Table. 16). So, 200 clocks are sufficient as a time limit of searching peak.

Gas	E [kv/cm](gap)	P [Torr]	T [°C]	vd[cm/μs]	longitudinal diffusion constant [$\mu m/\sqrt{cm}$]	transverse diffusion constant [$\mu m/\sqrt{cm}$]
$ArCO_2$ 70/30	0.6(drift)	760	20	1.5	147	130
$ArCO_2$ 70/30	2.1(transfer)	760	20	6.4	149	227
$ArCO_2$ 70/30	4.2(induction)	760	20	7.4	149	257

Table 16: Results of the calculation by Magboltz.

After obtaining the peak value of each waveform for all the 32 readout strips, the strip which has the largest peak value is selected and called "*max strip*". If the peak value of *max strip* was under the threshold, such events have no hits.

Making charge cluster

All the strips which exceed the threshold are picked up to make a "*cluster*". Since the ionized electrons diffuse, ionized charge spreads over several strips. So hit strips should be grouped to derive the hit position of GEM. The group is called *cluster*. The method to make a *cluster* is as following.

1. The strips which exceed the threshold are called "*hit strip*s".

2. *hit strip*s are grouped as a cluster if following condition is fulfilled.

$$a_{i+1} - a_i \leq n \quad (i = 1, 2 \ldots N-1, n \geq 1)$$

a_i is the strip number of *hit strip*. N is the number of *hit strip*s. n is a parameter input by hand. The number of strips contained in a *cluster* changes according to n. If $a_{i+1} - a_i > n$, a_{i+1} and a_i belong to different *cluster*s. $n = 2$ is used for 350 μm pitch readout and $n = 1$ for 700 μm pitch readout.

Then, a *cluster* which includes *max strip* is selected. It is called $cluster_{max}$. The hit position of GEM is calculated with the strips in $cluster_{max}$.

charge sum is defined as a sum of the peak values of the strips in $cluster_{max}$. It is expressed as,

$$\begin{aligned} charge\ sum &= \sum_{i=a_1}^{a_{N_{max}}} Q_i^{peak} \\ a_i &\in cluster_{max} \end{aligned}$$

a_i is a strip which belongs to $cluster_{max}$ and N_{max} is the number of strips in $cluster_{max}$. Q_i^{peak} is the peak value of ADC of the strip i. If *charge sum* was under the threshold, such events have no hits.

5.4.3 Additional cut

- **Cut of noisy strips of GEM**

  Noisy channels of GEM are recognized by the correlation between the hit position of GEM and SSDs. Noisy strips worsen the position resolution if it is over the threshold and included in $cluster_{max}$.

  The correlation between *max strip* of GEM and the hit position interpolated by SSDs are shown in Fig. 48. Strip No.15 and 17 of GEM are noisy. Fig. 49 shows the distribution of ADC value of an ordinary strip and a noisy strip.

  The left of Fig. 50 shows the residual distribution before the cut of noisy strips. Residual is defined as $x_{GEM} - x_{SSD}$. x_{GEM} is the hit position calculated with the strips of GEM and x_{SSD} is the interpolated position. There is a bump far from the center in the left of Fig. 50. After excluding the noisy strips from the process to determine the *max strip*, the bump disappeared (the right of Fig. 50). So the bump is considered to be caused by mistaking a noisy strip for *max strip*. However, the tail in the right side seems to increase before noisy strip cut. It is due to the dead strips. No13, 16, 18, 19 are the dead strips as seen in Fig. 48. The hit correlation under $|x_{GEM} - x_{SSD}| > 0.6$ is shown in the right of Fig. 51. The correlation at *max strip*=14, 20 which are next to the dead strips strongly remains. If a charge cluster overlaps the dead strips region, the strips which are next to the region are likely to be mistaken for *max strip* and make tail.

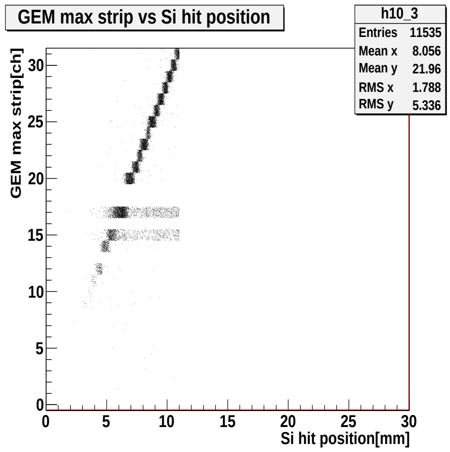

Figure 48: Hit position correlation between GEM and SSD: Noisy strips of GEM are seen as non-correlated events. Strip No.15,17 are noisy. No.13,16,18,19 are the dead strips.

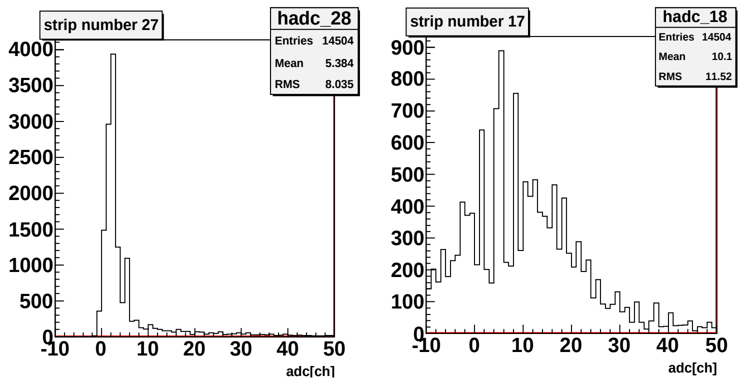

Figure 49: (left) Ordinary distribution of ADC value of one strip, (right) ADC distribution of a noisy strip.

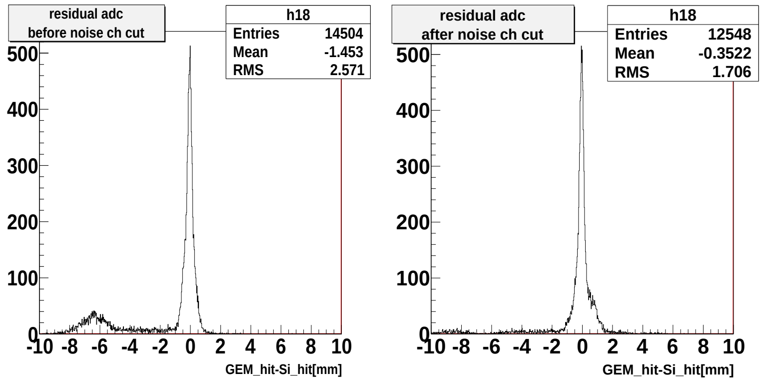

Figure 50: (left) The residual before noisy strip cut. (right) After noisy strip cut.

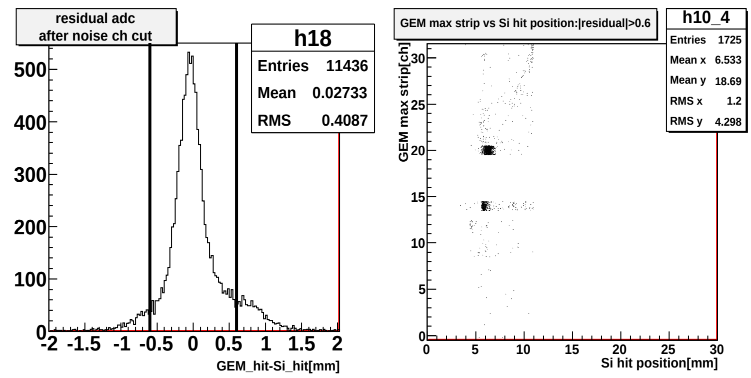

Figure 51: (left) The zoomed figure of the right of Fig. 50. (right) The correlation between the GEM max strip and the hit position calculated by SSDs of the events $|x_{GEM} - x_{SSD}| > 0.6$ mm in the left figure. The strips which are next to the dead strips or the noisy strips remain in the correlation.

- **GEM fiducial cut**

  Dead strips area of GEM is avoided according to the interpolated hit position. The aim of this cut is to remove the effect of dead channels and select fiducial area. Dead strips make tail in the residual distribution and worse the resolution because whole charge distribution can not be seen due to the dead strips (bottom left of Fig. 52). Tail is reduced by the fiducial cut to the interpolated hit position.

  The top of Fig. 52 is the hit correlation between GEM and interpolated hit position. The bottom right of Fig. 52 is a residual distribution after the cut of $x_{SSD} > 7$ and it is shown that the tail is reduced.

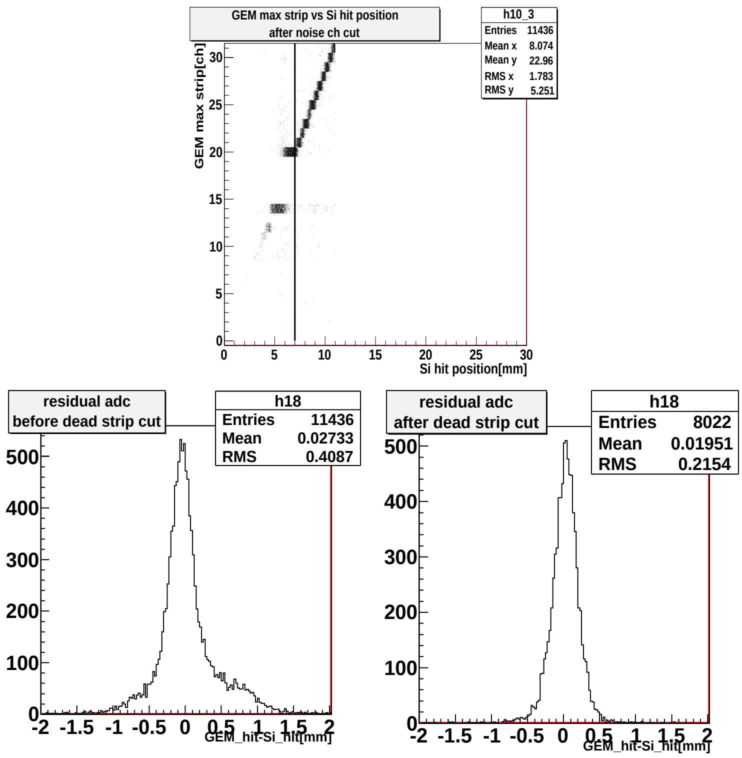

Figure 52: (top) Hit position correlation between GEM and SSDs. The effect of the dead strips appear at strip No.14 and 20. (bottom left) Residual before the cut of dead strips, (bottom right) After the dead strips cut.

5.4.4 GEM hit position analysis

4 methods are used to calculate the hit position of GEM. Charge information is used for 0° beam and timing information is used for 15° and 30° inclined beam.

1. **Center of charge(COC) method**

   This method calculates the hit position by the weighted mean of charge. Hit position x_{GEM} is calculated as following.

   $$x_{GEM} = \sum_{i=a_1}^{a_{N_{max}}} p \times a_i \frac{Q_i^{peak}}{\sum_{j=a_1}^{a_{N_{max}}} Q_j^{peak}}$$

   a_i is the strip number in $cluster_{max}$ and N_{max} is the number of strips in $cluster_{max}$. p is the strip pitch of readout, 350μm or 700μm.

   Center of charge method is expected to be effective for 0° beam because ionization points do not spread along the track. But the resolution deteriorates for the inclined beam because charge cluster spread along a track and the amount of charge does not tell the hit position (Fig. 53).

2. **Middle point method**

   By middle point method, hit position is given by

   $$x_{GEM} = p \times \frac{a_1 + a_{N_{max}}}{2}$$

   The position resolution by middle point method is expected to be worse than COC method, however the amount of charge is not necessary to calculate the hit position. So middle point method does not need ADC in readout electronics.

3. **Timing fit method**

   Timing method uses the difference of the drift time among the strips. The drift time is defined as the number of FADC clocks from trigger timing to the timing at which the signal exceeds a half of its peak value. The difference of the drift time among the strips corresponds to the difference of the ionization points along beam axis. So the relative position perpendicular to the readout plane is reconstructed if drift velocity was selected properly.

   The ionization point along beam axis is expressed as following,

   $$z_{a_i} = vd \times t_{a_i}$$

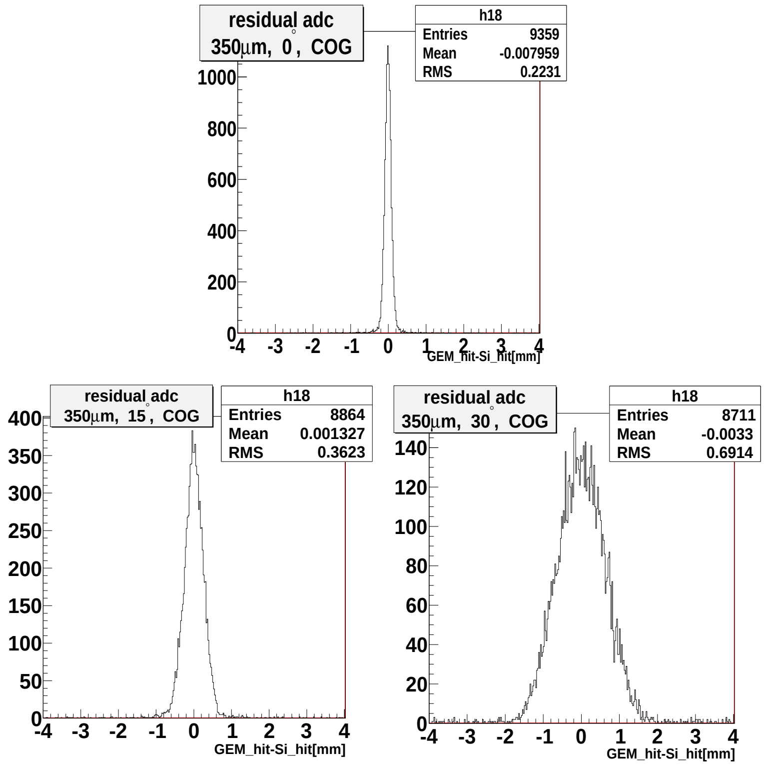

Figure 53: Residual distribution calculated by center of charge method. (top) 0° beam, (bottom left) 15° beam, (bottom right) 30° beam. Residual calculated by COC method deteriorates according to the angle.

t_{ai} is the drift time of strip a_i which belongs to $cluster_{max}$. vd is drift velocity. The track is derived by fitting the points ($p \times a_i$, za_i) with a linear function. p is the strip pitch. If the formula of the track is obtained as $z = Ax + B$, x_{GEM} is calculated as following. z is the direction perpendicular to readout plane and x is the direction in which strips read the hit position.

$$x_{GEM} = \frac{z_{ref} - B}{A}$$

Here z_{ref} is a parameter input externally and determined as the mean value of $|x_{GEM} - x_{SSD}|$ comes to zero. Event display is shown in Fig.56.

Residual is scanned by drift velocity vd to find the optimum point (Fig. 54). In Fig. 54, best resolution is achieved at $vd = 2.2\ cm/\mu s$. The incident angle θ is reconstructed by the gradient of the track obtained by fitting.

$$\theta\ [^\circ] = 90 - \arctan(A)/\pi \times 180$$

The distribution of θ is the right of Fig. 55. The peak of calculated angle distribution is about 16° and this is consistent with the setup of analyzed data.

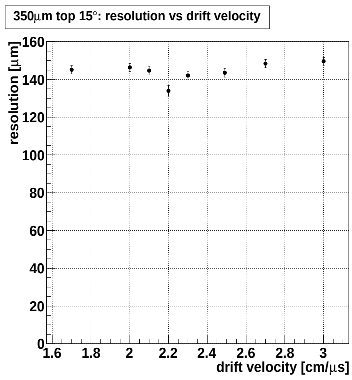

Figure 54: Residual vs drift velocity by timing fit method. Strip pitch is 350 μm and incident angle is 15°. vd=2.2 cm/μs is the optimum point.

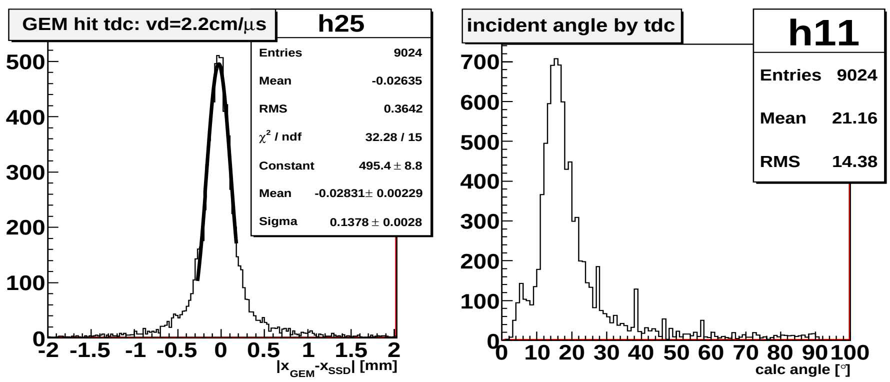

Figure 55: (left) The residual distribution at vd=2.2 cm/μs. (right) The calculated angle distribution of 15° run. vd=2.2 cm/μs.

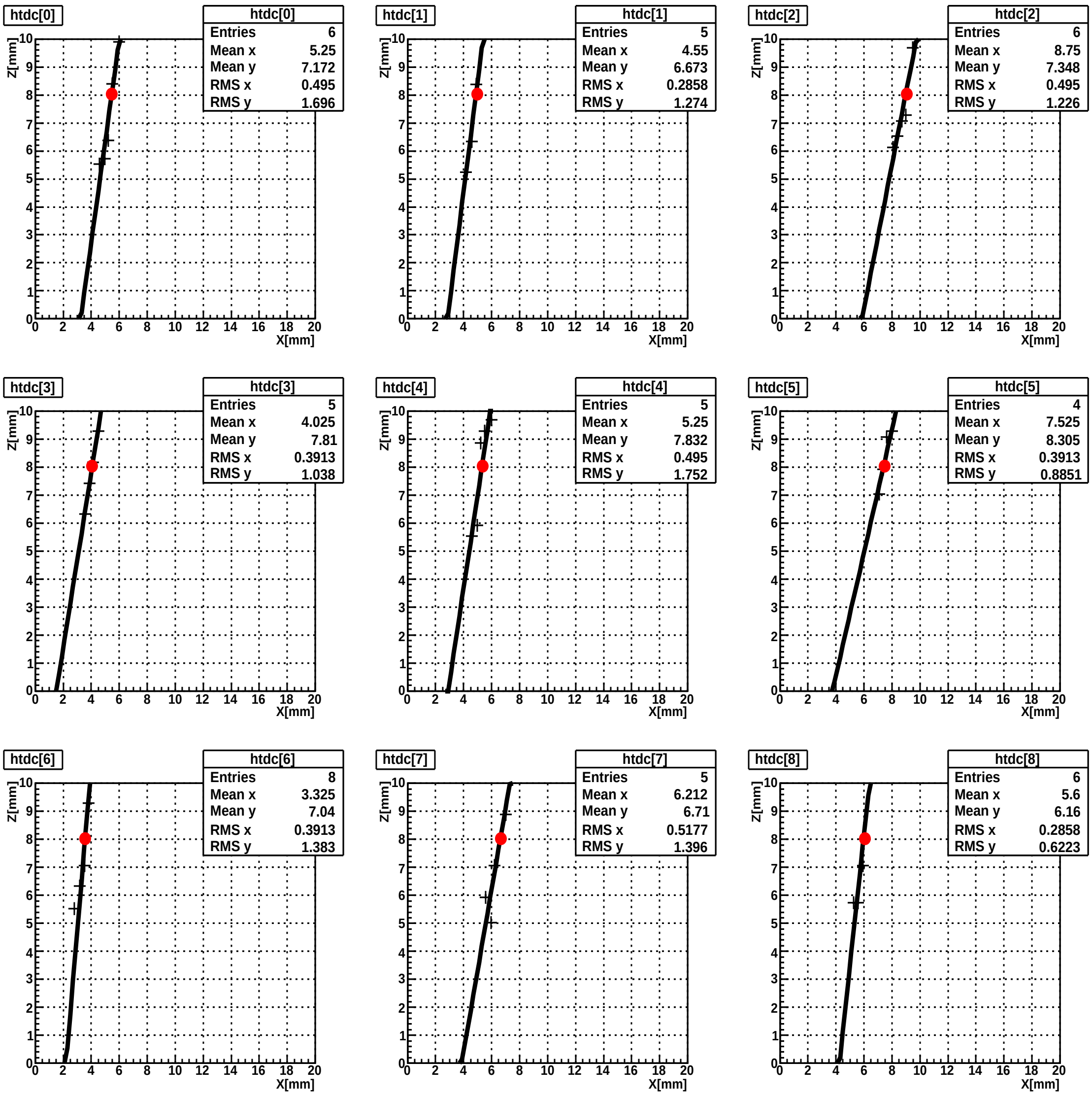

Figure 56: Event display of tdc fit method(15° run). Cross points: GEM hit position., Red point: hit position interpolated by SSDs., Line: track derived by fitting points. vd=2.2cm/μ s.

4. **Fixed angle timing method**

   Timing fixed angle method fixes the gradient of the calculated track to the incident angle when fitting. So the gradient is 15° or 30°. The gradient of track is expected to be given by other 2 GEM chambers in the real experiment.

Estimation of tracking accuracy

Tracking accuracy δx is estimated by the resolution of SSD (σ_{SSD}) and the multiple scattering effect between GEM and SSD2 (σ_{MS}). The hit position interpolated by SSDs are calculated as following,

$$x = \frac{145 \cdot x_{SSD1} + 130 \cdot x_{SSD2}}{275}$$

x_{SSD1} and x_{SSD2} are the hit positions of SSD1 and SSD2. So the accuracy of x is,

$$\begin{aligned}
\delta x &= \sqrt{(\frac{145}{275})^2(\delta x_{SSD1})^2 + (\frac{130}{275})^2(\delta x_{SSD2})^2} \\
\delta x_{SSD1} &= \sigma_{SSD} = 80/\sqrt{12} \sim 23\mu m \\
\delta x_{SSD2} &= \sqrt{\sigma_{SSD}^2 + \sigma_{MS}} \\
&= \sqrt{23^2 + 59^2} \sim 63\mu m
\end{aligned}$$

σ_{MS} is estimated by the radiation length of air and GEM. Thus δx is,

$$\delta x \sim 32\mu m$$

The position resolution of GEM is calculated as $\sigma_{GEM}[\mu m] = \sqrt{\sigma_{residual}^2 - 32^2}$. σ_{GEM} is the width of residual distribution.

5.4.5 GEM efficiency calculation

The efficiency of GEM tracker ε is expressed as following.

$$\varepsilon = \frac{N_{total} - N^{SSD}_{invalid} - N^{SSD}_{double} - N^{SSD}_{window} - N^{GEM}_{invalid} - N^{GEM}_{far}}{N_{total} - N^{SSD}_{invalid} - N^{SSD}_{double} - N^{SSD}_{window}}$$

The meaning of each number is as follows.

- N_{total}

  The number of total events.

- $N^{SSD}_{invalid}$

  The number of events in which at least one SSD has no hit. Hit is defined by the significance value of ADC.

- N^{SSD}_{double}

  The number of events in which at least one SSD has double hit.

- N^{SSD}_{window}

  The number of events in which the beam hits SSDs but not GEM geometrically.

- $N^{GEM}_{invalid}$

  The number of events in which the ADC value of *max strip* is under the threshold.

- N^{GEM}_{far}

  The number of events in which $|x_{SSD} - x_{GEM}| \geq 1$mm. x_{SSD} is the hit position interpolated by SSDs and x_{GEM} is the hit position of GEM.

5.5 Results

All the data sets taken at the beamtest are shown in Table. 17. From these data, we focus on following points,

- **The operation of 200×200 mm^2 and 300×300 mm^2 GEM**

  Gain and position resolution are the benchmarks for the performance.

- **Position resolution and efficiency**

- **The position resolution of y-strip**

  Readout strips are merged in offline analysis to investigate the position resolution with coarse pitch.

- **Position resolution for 15° beam without waveform information**

GEM size[mm]	strip pitch[μm]	read direction	drift gap[mm]	drift field[V/cm]	V_{GEM}[V]	angle[°]
100	350	x	6	600	410	0
100	350	x	6	600	410	15
100	350	x	6	600	410	30
100	350	y	6	600	410	0
100	350	y	6	600	410	15
200	700	x	6	600	420	0
200	700	x	6	600	430	0
200	700	x	6	600	420	15
200	700	x	6	600	430	15
200	700	x	6	600	420	30
200	700	x	6	600	430	30
200	700	y	6	600	430	0
300	700	x	6	600	420	0
300	700	x	6	600	420	15
300	700	x	6	600	420	30
300	700	y	6	600	420	0
300	700	y	6	600	420	15

Table 17: Tested set ups. V_{GEM} is the potential between the electrodes of every GEM foil. The polyimide between x-strips and y-strips is excluded in 350μm pitch readout but not in 700μm pitch.

5.5.1 Operation of large GEM

The distributions of charge sum and the residual for 0° beam calculated by center of charge method are shown in Fig. 57 according to GEM size. The gap length of the setups of all the figures are 6, 2, 2 and 2 mm which corresponds to the drift gap, upper transfer gap, lower transfer gap and inductin gap. Please note that $100\times100\mathrm{mm}^2$ GEM is operated with 350μm pitch readout however 200×200 and $300\times300\mathrm{mm}^2$ GEM are operated with 700μm pitch readout.

The peak of charge sum distribution corresponds to the gain and they are shown in Table.18. Each distribution is fitted with Landau distribution. Gain is estimated as following,

$$\begin{aligned} n_{seed} &= (\frac{dE_{Ar}}{dx}\cdot 0.7 + \frac{dE_{CO_2}}{dx}\cdot 0.3)[eV/cm] \times 0.6[cm]/28[eV] \sim 60 electrons \\ n_{signal} &= MPV[ch]\cdot\frac{1}{256}[V/ch]/(3.2[V/pC]\cdot 1.6\times10^{-7}[pC]) \\ gain &= \frac{n_{signal}}{n_{seed}} \end{aligned}$$

n_{seed} is the number of ionized electrons by e^+ beam. $\frac{dE_{Ar}}{dx}$ and $\frac{dE_{CO_2}}{dx}$ are calculated from the values of Particle Data Group[25] and ~2.5 KeV/cm and 3.4 KeV/cm. 0.6 cm is the length of drift gap and 28 eV is the working function of $ArCO_2$(70/30)[16]. n_{signal} is the charge of signal expressed as the number of electrons. MPV is derived by the Landau fitting(Fig. 57). 1/256 [V/ch] is determined by the spec of FADC and 3.2 V/pC is the gain of pre-amp.

The gain of large GEM is about 1/3 of the 100×100 mm^2 GEM. One of the causes is the field strength. But the difference of gain can not be explained only by the field configuration.

Although the gain of large GEM is lower and their strip pitch is coarser, the residual for 0° by center of charge method are not so worse compared to 100×100 mm^2 GEM. Since the tracking accuracy of SSDs and multiple scattering as ~32 μm, the resolution for 0° of 100×100 mm^2, 200×200 mm^2 and 300×300 mm^2 are 75, 88 and 79 μm.

So large GEM are operated stably and have almost same resolution as the past GEM. The question about the difference of gain remains and we suspect the gas condition and the mechanical structure of a chamber as the cause. A new chamber is being prepared which is made of metal and more gas tight.

Gap name	100×100 mm^2	200×200 mm^2	300×300 mm^2
E_D [kV/cm]	0.6	0.6	0.6
E_{T1} [kV/cm]	4.1	2.1	2.1
E_{T2} [kV/cm]	4.1	2.1	2.1
E_I [kV/cm]	4.1	4.2	4.2
V_{GEM} [V]	410	420	420
gain	16000	4800	5200

Table 18: Configuration of electric field of each gap. E_D denotes the electric field in drift gap, E_{T1} is the transfer gap near top, E_{T2} is the transfer gap near bottom and E_I is the induction gap.

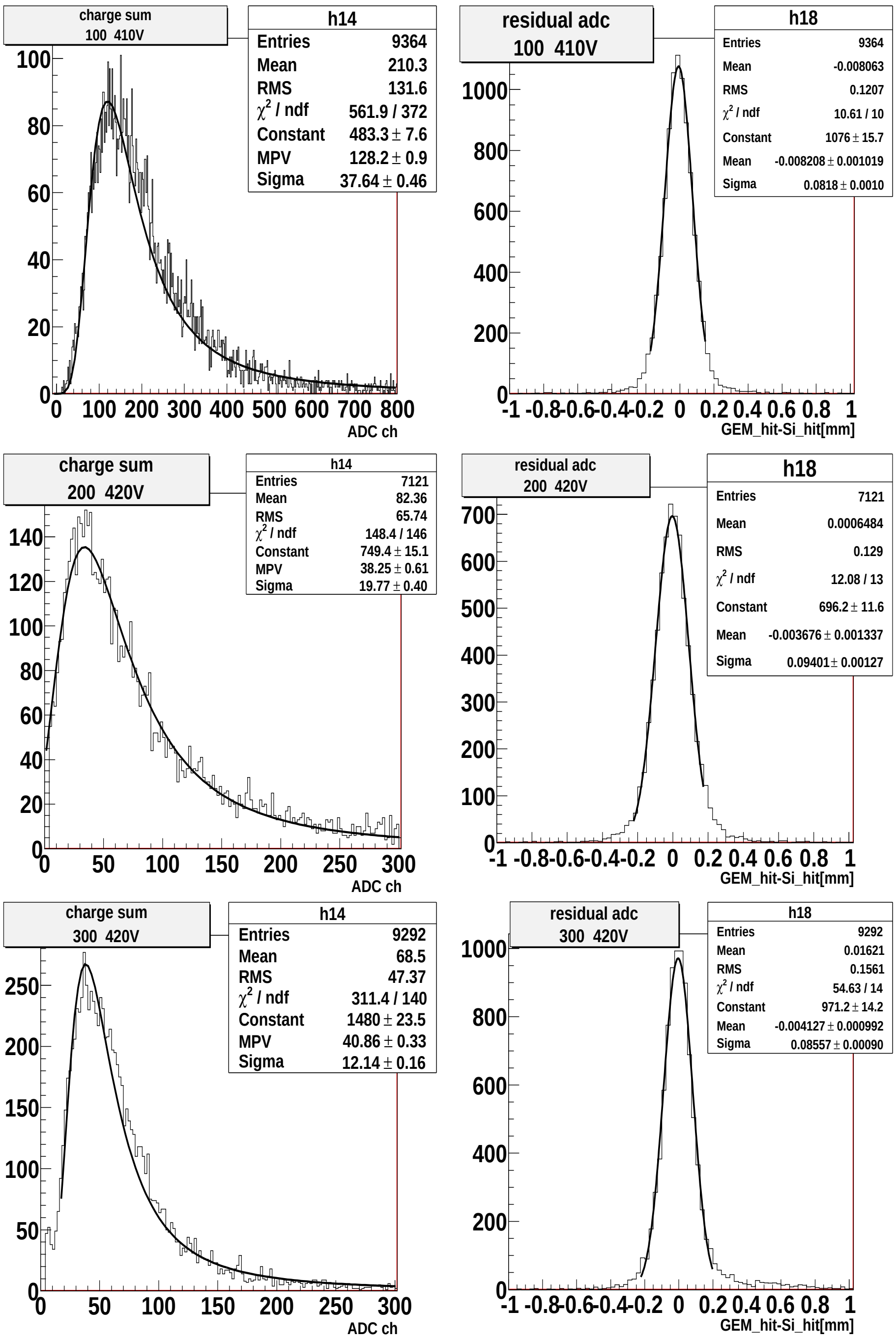

Figure 57: Charge sum and residual calculated by center of charge method: (top) 100×100, (middle) 200×200, (bottom) 300×300mm^{2}GEM

5.5.2 Position resolution and efficiency

The goal of the position resolution based on the results of Monte-Carlo simulation is **100 μm up to 15° inclined beam**.

Fig. 59∼62 are the position resolution of each setup. They are distinguished by the strip pitch and the direction of strip. 'top' means horizpntal strips and 'bottom' means vertical strips. The best resolution is in Table. 19.

strip pitch and direction	0°		15°	30°
	COC	Middle		
350 μm-X	77	122	105	127
700 μm-X	79	184	166	235
350 μm-Y	134	159	182	
700 μm-Y	175	257	341	

Table 19: Position resolution

The best position resolution for 15° and 30° are derived by fixed angle timing method. From Table. 19, it is necessary use 350 μm pitch readout in horizontal direction to achieve the resolution of 100 μm up to 15°.

The obtained position resolution and mass resolution calculated by simulation for each method are shown in Table. 20 and Fig. 58.

data set	horizontal resolution [μm]						vertical (middle) [μm]	ΔM [MeV/c^2]	ΔM ($\beta\gamma_\phi$ < 1.25) [MeV/c^2]
	0°		15°		30°				
	COC	middle	tdc fit	tdc fix	tdc fit	tdc fix			
1	77			105		127	255	5.9	4.8
2	77		140		143		255	6.4	4.9
3		122	140		143		255	7.4	5
4		122	245 (middle)		368 (middle)		255	9.3	6.3

Table 20: Obtained position resolution and calculated mass resolution for each analysis method.

The results of TDC method in Table. 20 are derived with the information of pulse shape. So it is difficult to achieve mass resolution of 5 MeV/c^2 only with hit information for each strip. Thus, the requirement for readout configuration is **to know the timing of the peak of signal.**

The resolution of 100 μm is not achieved by middle point method for 0° beam. Further analysis about 0° and middle point method is needed.

The efficiency of each analysis method is shown in Fig. 63∼66. The efficiency becomes worse as the incident angle increases. And the efficiency

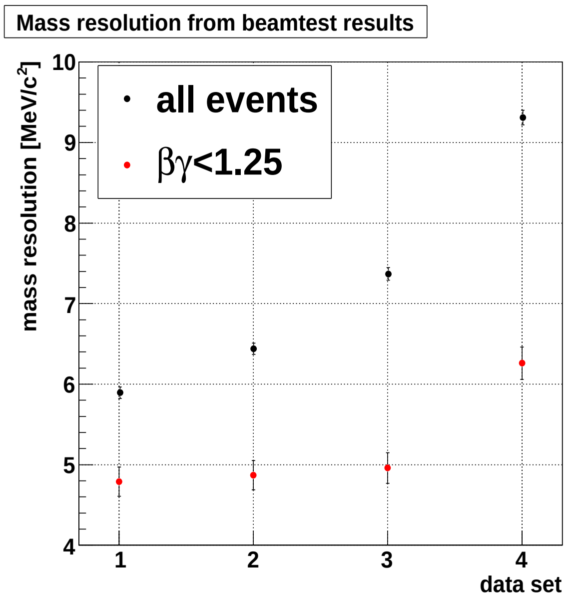

Figure 58: Mass resolution obtained by simulation with the position resolution of beamtest results. X-asis is the number of "data set" in Table. 20.

of the bottom side is worse than the top side. This is considered due to the difference of the pulse height of the top side and the bottom side. The signal to noise ratio (S/N) ratio in the bottom side is discussed next.

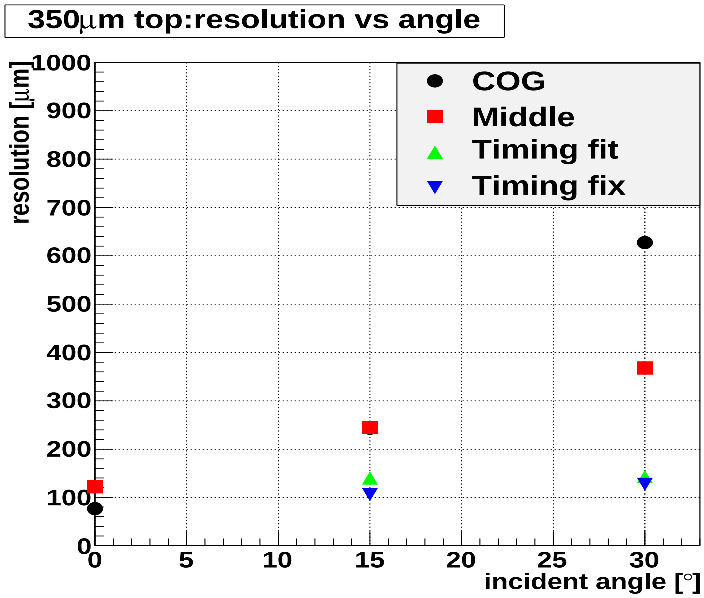

Figure 59: Position resolution vs incident angle:350 μm pitch, top side.

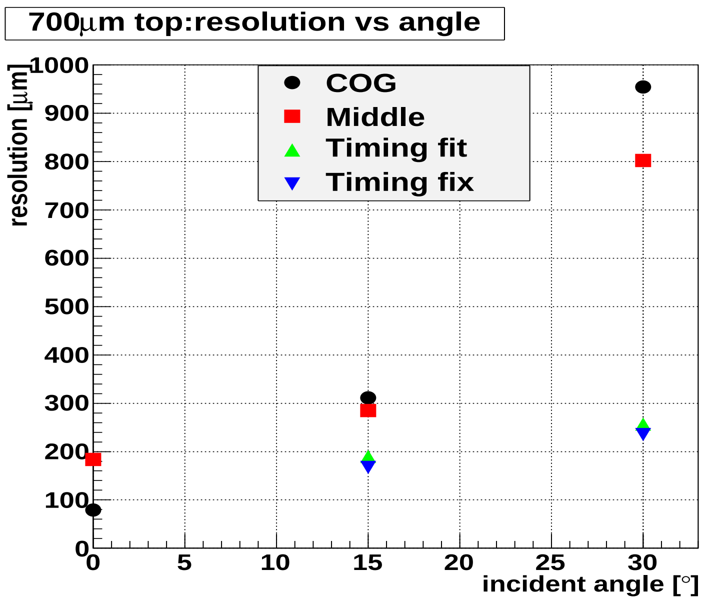

Figure 60: Position resolution vs incident angle:700 μm pitch, top side.

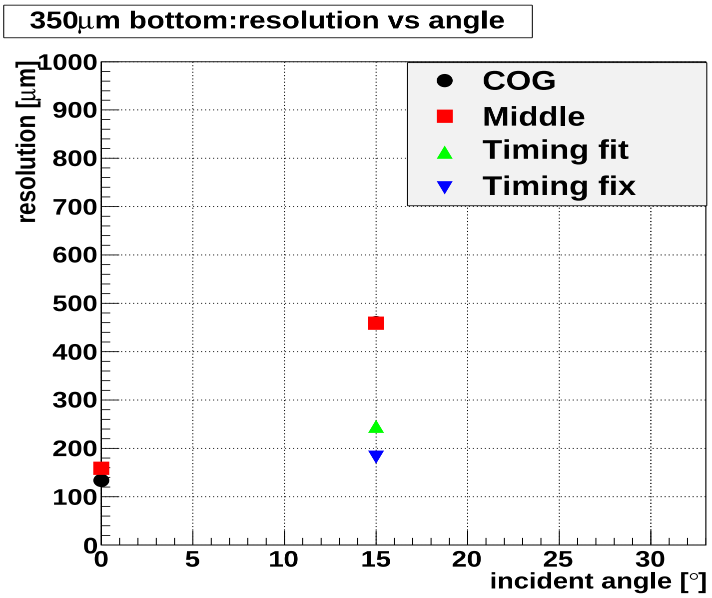

Figure 61: Position resolution vs incident angle:350 μm pitch, bottom side.

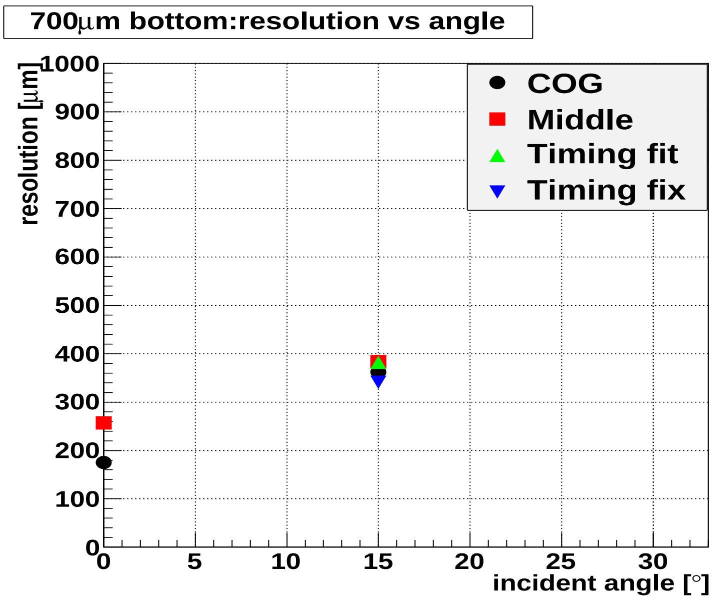

Figure 62: Position resolution vs incident angle:700 μm pitch, bottom side.

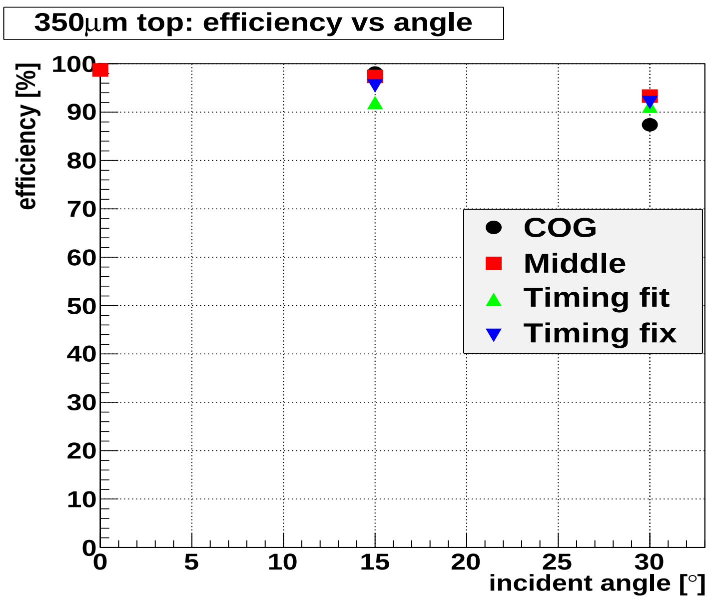

Figure 63: Efficiency vs incident angle:350 μm pitch, top side.

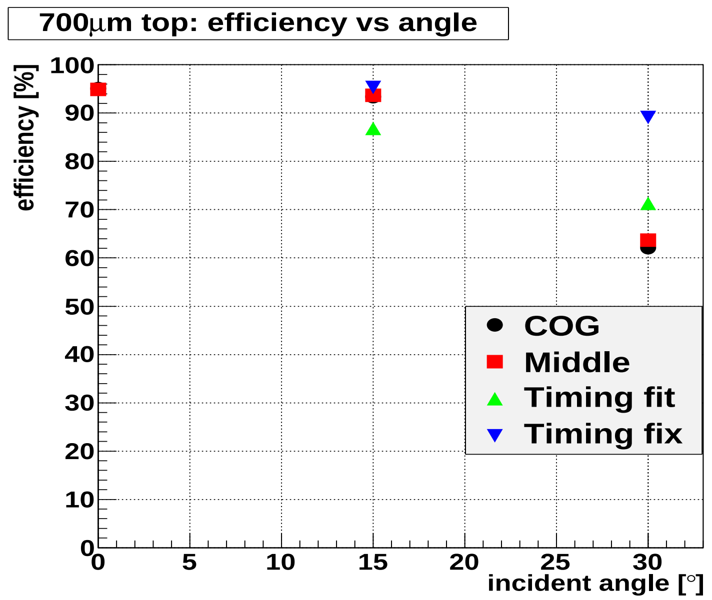

Figure 64: Efficiency vs incident angle:700 μm pitch, top side.

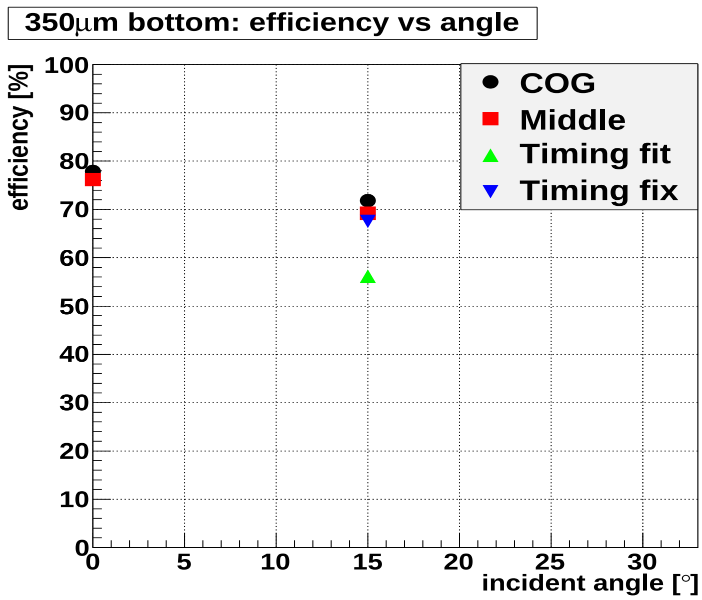

Figure 65: Efficiency vs incident angle:350 μm pitch, bottom side.

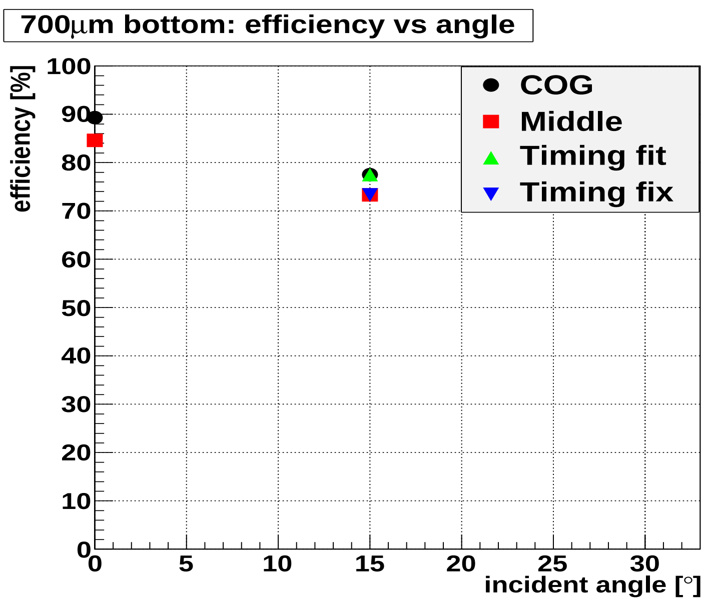

Figure 66: Efficiency vs incident angle:700μm pitch, bottom side.

5.5.3 Resolution of the bottom side

The position resolution of the vertical strips is important to determine the strip pitch of the bottom side readout. From simulation results, Mass resolution degrades no more than 0.5 MeV/c^2 even if position resolution in vertical direction degrades from 200 μm to 700 μm. 350 μm and 700 μm pitch readout in the bottom side are tested in the beamtest and residual of 270 μm is achieved with 700 μm pitch for 0° beam by middle point method (Fig. 62). So 700 μm pitch readout in the bottom side has enough resolution. The position resolution with 1400 μm pitch is evaluated by offline analysis to consider the capability of decreasing the number of readout channels in the bottom side.

Resolution of 1400 μm pitch

The data of 700 μm pitch for 0° beam is analyzed as following because 0° inclined electrons are expected to be dominant in the E16 experiment. The FADC value of every two strips are combined to regard 700 μm pitch as 1400 μm pitch as following.

$$fadc'[i][j] = fadc[2i][j] + fadc[2i+1][j]$$

Here i denotes the strip number 0, 1, 2...16 and j is the clock of FADC from 0 to 640 ch. 1 ch is 10 ns. *fadc'*[i][j] show the FADC value of 1400 μm pitch and *fadc*[i][j] are the ADC value of 700 μm pitch which are measured in the beamtest. Pedestal for 1400 μm pitch is calculated same as FADC value and subtracted. The max value of FADC is determined by comparing the pulse height clock by clock for all 16 strips and they are called as *peak value* of each strip. Then the *peak value*s are compared among the strips and max ADC strip of the event is determined. If the max ADC strip was over the threshold, cluster is formed by the max strip and its neighbor strips which are over the threshold. The hit position on GEM is calculated by the middle point method in the cluster.

$$(\textbf{hit position(GEM)}) = 1400\mu m \times \frac{(a_0 + a_N)}{2}$$

a_0 and a_N are the strip numbers of both ends of the cluster. The residual is calculated as the difference of the hit position on GEM and the hit position determined by SSDs. The residual of before and after gathering strips is shown in Table. 21 and Fig. 67.

The efficiency is quite lower than the top side. This is considered to be due to the bad S/N ratio of the bottom side. The pulse height of the bottom side is lower than the top side.

	before	after
strip pitch [μm]	700	1400
resolution [μm]	266	423
efficiency [%]	87	74
threshold [ch]	5	9

Table 21: Resolution and efficiency before and after merging strips.

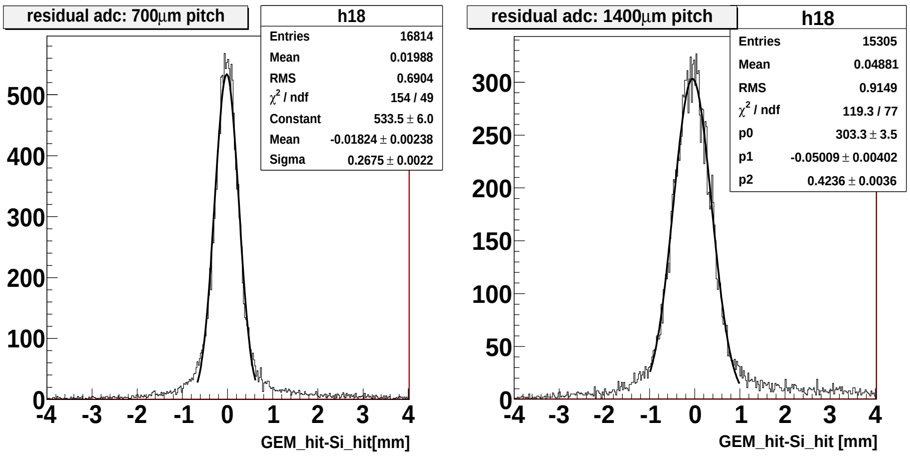

Figure 67: (left) Residual of 700 μm pitch. (right) Residual of 1400 μm pitch.

Estimation of S/N

S/N is estimated by the sum of peak values of the strips in a cluster.

$$S/N = \frac{\sum_{i=1}^{N} Q_{a_i}^{peak}}{(\sum_{i=1}^{32} Q_i^{peak} - \sum_{i=1}^{N} Q_{a_i}^{peak}) \times N/(32-N)}$$

N is the number of strips in a cluster and a_i is the strip number of the strips in a cluster. So numerator is the sum of peak values of the strips in a cluster. Denominator is the sum of the peak values of the strips which are not included in the cluster and normalized to the number of strips in a cluster, N. 32 is the total number of strips.

The comparison of S/N between 700 μm (before merging strips) and 1400 μm (after merging) is shown in Fig. 68. Black line shows the S/N of 700 μm pitch and red line is 1400μm pitch. The S/N of 1400 μm pitch is slightly worse since noise becomes about twice but signal does not become twice after adding the fadc values of every two strips. So the efficiency of 1400 μm pitch is expected to be worse than the 700 μm pitch (Table. 21).

The comparison between 700 μm pitch top side and 700 μm pitch bottom side is shown in Fig. 69. S/N of $\sim$10 is achieved in top side in contrast to $\sim$3 in 700 μm pitch bottom side run. The configuration of the electric field is the same for both run. The cause of small pulse height of the bottom side is considered due to the kapton of 25 μm thickness between the top side and the bottom side strips. It is now planned to make a new readout in which thinner kapton (12.5 μm thickness) is used.

Conclusion

Position resolution of 420 μm is achieved with 1400 μm pitch strips in the bottom side. So it is possible to decrease the number of the strips from a view point of resolution, but the efficiency is quite low. Low efficiency has roots in low S/N ratio and efficiency will be improved by thinning the material between the top side and the bottom side of the readout and making the pulse height bigger.

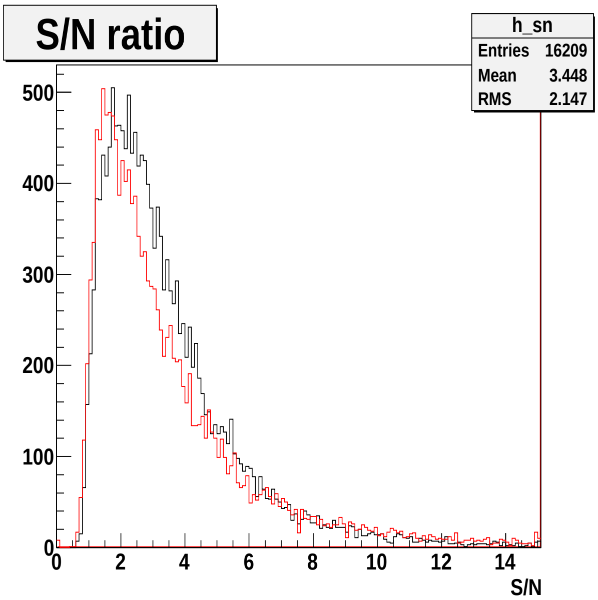

Figure 68: S/N ratio. (black) 700μm pitch. (red) 1400μm pitch.

5.5.4 Analysis without waveform information

Position resolution is evaluated without the information of waveforms to consider the case in which readout electronics is only comparator and clocks. The past analysis uses the peak values of waveforms in COC method and

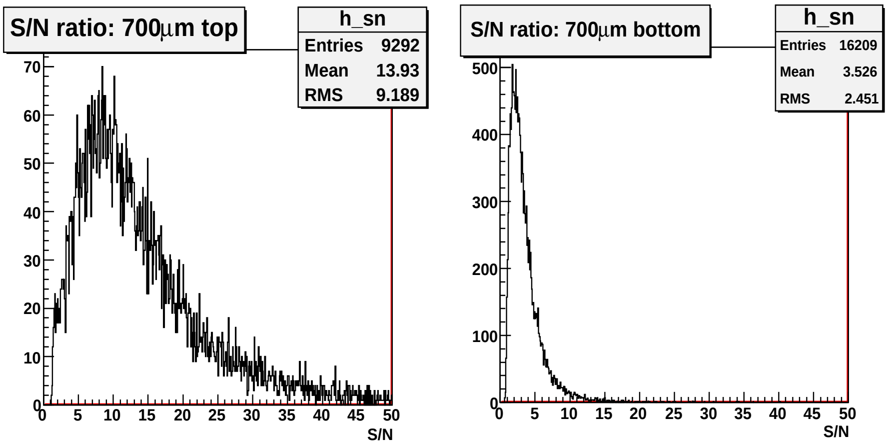

Figure 69: (left) S/N of 700μm pitch top side. (right) S/N of 700μm pitch bottom side.

the timing at a half of the peak in timing method. But only the timing at which the signal exceeds a threshold value can be known without ADC since the peak position of signal is unknown.

Resolution is derived with the following assumptions:

- **The peak value of each strip's ADC is unknown.**
- Sum of signal charge is unknown.
- Max ADC strip is unknown.
- The timing of the peak is unknown.

Since max ADC strip is unknown, the method to make a cluster changes from the past analysis. Specific procedure of analysis is as following,

1. Threshold value which is common for all the strips is set.
2. The height of each waveform is compared with the threshold clock by clock up to 200 clocks(=2 μs) for one strip. It is repeated for all the 32 strips.
3. If the waveform of a strip exceeds the threshold, that strip is counted as "*ring_strip*" .
4. If the *ring_strip*s were in series, they are grouped as a "*cluster*". "n_allow" is a parameter of the number of strips which are not in series

but allowed to be included in a cluster. For example, *n_allow*=0 and *ring_strips* are 1, 2, 4 and 5, the *clusters* are (1,2) and (4,5). However, if *n_allow*=1, the *cluster* is (1,2,4,5). Setting *n_allow* is effective when there is a dead strip.

5. Select a *cluster* which contains the largest number of strips. In past algorithm, the *cluster* which contains *max strip* was selected.

6. Middle point method is used in the largest cluster to calculate the hit position on GEM for 0° beam. Timing fix method is used in the largest cluster for 15° beam.

Results: For 0° beam

Middle point method is used to derive the hit position on GEM for 0° beam data. The residual and efficiency against threshold are shown in Fig. 70. 16 seems the best value of the threshold for residual and efficiency. Residual 119 μm and efficiency 98.6% is achieved. The residual and efficiency by past algorithm are 121 μm and 98.7%. So the selection of the cluster works well in new algorithm which selects the largest cluster.

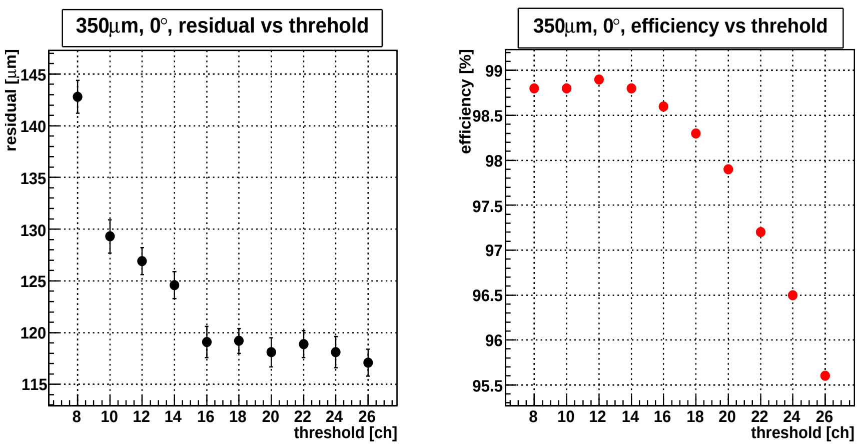

Figure 70: 350μm pitch, 0° analysis. (left) Residual vs threshold, (right) Efficiency vs threshold.

Results: For 15° beam

Timing fix method is used for 15° beam. First, residual is scanned by the threshold value(Fig. 71 (left)). Drift velocity is fixed as 1.5cm/μs. The best residual is 156 μm at (threshold)=9.

The residual is scanned by drift velocity (Fig. 72). 145 μm is achieved at 1cm/μs and efficiency is 98.7%. The residual by past algorithm which uses the timing of a half of a peak is 117 μm. One of the reasons for the degradation of the resolution is considered to be the pulse height dependece of the timing and now being analyzed.

Conclusion

Good position resolution $\sim$ 115 μm is obtained by threshold method for 0° beam, but resolution 100 μm is not achieved for 15° beam. The improvement of the resolution for 15° will be possible by correcting the timing at which a signal exceeds the threshold with pulse height of pulse width.

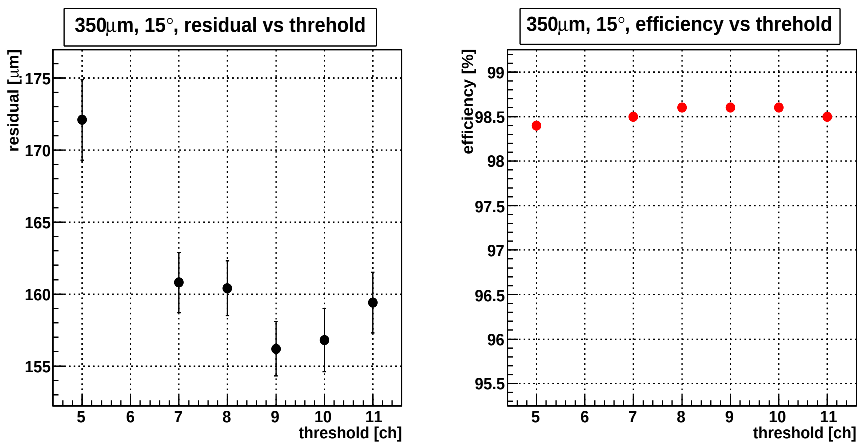

Figure 71: 350μm pitch, 15° analysis. (left) Residual vs threshold, (right) Efficiency vs threshold. Drift velocity is 1.5cm/mus.

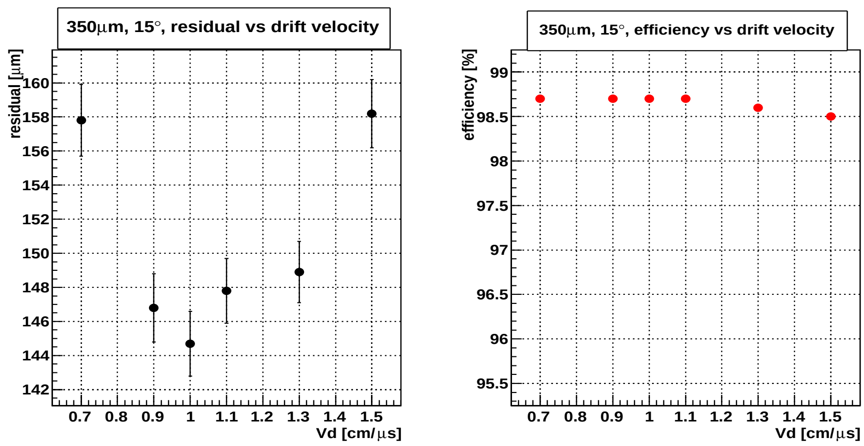

Figure 72: 350μm pitch, 15° analysis. (left) Residual vs drift velocity, (right) Efficiency vs drift velocity

5 Conclusions & Outlook

Two points have been focused in this thesis for the development of GEM tracker. They are the development of large GEM and the determination of readout configuration.

Development of large GEM

200×200 mm^2 and 300×300 mm^2 GEM are developed and their performance are evaluated in the beamtest. The gain of $\sim 10^4$ is achieved by the improvement of hole size and flabbiness in large GEM.

The position resolution of large GEM is also evaluated in the beamtest. Resolution of 80 μm is achieved for 0° beam by center of charge method with large GEM. It is almost the same performance as 100×100 mm^2 GEM. The tests for resolution with 350 μm pitch readout and for gain should be proceeded.

Readout configuration

The required position resolution is estimated by the Monte-Carlo simulation. The position resolutuion for $0^\circ \sim 15^\circ$ inclined electrons and the vertex position resolution are important for mass resolution. Mass resolution is estimated as 4.6 MeV/c^2 with horizontal resolution of 100 μm up to 15° inclined beam and vertex resolution of 100μm.The resolution with 350 μm pitch and 700 μm pitch readout are evaluated in the beamtest.

For the top side, the use of 350 μm pitch readout is necessary to achieve 100 μm up to 15° inclined particles.

For the bottom side, 700 μm pitch and 1400 μm pitch readout achieves the resolution better than 500 μm and it fulfills the experimental requirement. The resolution of 1400 μm pitch is estimated by offline analysis. But S/N is less than 1/3 of the top side and efficiency is quite low ($\sim$80%). This is considered due to the mechanical structure of the readout. The use of thinner polyimide (12.5 μm thickness) between the top side and the bottom side is proposed as a solution.

Mass resolution is evaluated by Monte Carlo simulation with obtained position resolution. The timing of the peak of signal is important for inclined electrons and for mass resolution of 5 MeV/c^2. So front-end electronics is required to get the information of the peak of a pulse.

Acknowledgements

I would like to appreciate Prof. K. Ozawa for his patient support and appropriate advices. I also express my gratitude to Prof. H. Enyo and Dr. M. Sekimoto for their great advices.

I would like to appreciate Dr. S. Yokkaichi and Dr. K. Aoki for their kindness and gread support. I would like to thank Prof. H.Hamagaki, Dr. T. Gunji and Mr. Y. Hori for their support in beamtest. I also thank Dr. T. Ishikawa and Tohoku LNS group who enable us to use beam for the test experimetnt. I express my gratitude to Mr. Y. Watanabe for his great support and advices. And I also thank Mr. S. Masumoto, Ms. A. Takagi and Mr. K. Kannno who always support me.

At last, I thank may parents for allowing me to concentrate on the student life.

References

[1] Y.Nambu and G.Jona-Lasinio, Phys. Rev. **122**(1960) 345

[2] Y.Nambu and G.Jona-Lasinio, Phys. Rev. **124**(1961) 246

[3] Surikagaku, Science-sha, **9**(2010)

[4] T.Hatsuda and S.H.Lee, Phys. Rev. **C46**(1992)R34

[5] M.Naruki *et al.*, Phys. Rev. Lett. **96**(2006)092301

[6] R.Muto *et al.*, Phys. Rev. Lett. **98**(2007)042501

[7] B.A.Mecking *et al.*, Nucl. Instrum. Meth. A **503**(2003)513

[8] M.H.Wood *et al.*, Phys. Rev. C **78**(2008)015201

[9] P.Muehlich *et al.*, Phys. Rev. C **67**(2003)024605

[10] R.Nasseripour *et al.*, Phys. Rev. Lett. **99**(2007)262302

[11] S.Yokkaichi *et al.*, Proposal "Electron pair spectrometer at the J-PARC 50-GeV PS to explore the chiral symmetry in QCD"

[12] B.Ketzer *et al.*, Nucl. Instrum. Meth. A **535**(2004)314

[13] A.Kozlov *et al.*, Nucl. Instrum. Meth. A **523**(2004)345

[14] C.Aidala *et al.*, Nucl. Instrum. Meth. A **502**(2003)200

[15] F.Sauli, Nucl. Instrum. Meth. A **386**(1997)531

[16] F.Sauli, "Principles of operation of multiwire proportional and drift chambers", Lectures given in the academic training programme of CERN(1975-1976)

[17] A report by Raytech.Co. 2010/8/31.

[18] GEM check sheet by Raytech.Co.

[19] T.Uchida *et al.*, Gain measurement of triple GEM chamber 2006/1/27

[20] S.Bachmann *et al.*, Nucl. Instrum. Meth. A **438**(1999)376

[21] Y.Nara *et al.*, Phys. Rev. C **61**(1999)024901

[22] Y.Watanabe, Master thesys, University of Tokyo (2010)

[23] H.Yamazaki *et al.*, Nucl. Instrum. Meth. A **536**(2005)70

[24] S.F.Biagi, Nucl. Instrum. Meth. A **421**(1999)234

[25] http://pdf.lbl.gov/2006/reviews/passagerpp.pdf